© 2016. Published by The Company of Biologists Ltd | Development (2016) 143, 427-436 doi:10.1242/dev.130112

RESEARCH ARTICLE

Villification in the mouse: Bmp signals control intestinal villus patterning

Katherine D. Walton[1,*], Mark Whidden[2], Åsa Kolterud[3], Suzanne K. Shoffner[2], Michael J. Czerwinski[1], Juhi Kushwaha[1], Nishita Parmar[1], Deepa Chandhrasekhar[1], Andrew M. Freddo[1], Santiago Schnell[2,4] and Deborah L. Gumucio[1,*]

ABSTRACT

In the intestine, finger-like villi provide abundant surface area for nutrient absorption. During murine villus development, epithelial Hedgehog (Hh) signals promote aggregation of subepithelial mesenchymal clusters that drive villus emergence. Clusters arise first dorsally and proximally and spread over the entire intestine within 24 h, but the mechanism driving this pattern in the murine intestine is unknown. In chick, the driver of cluster pattern is tensile force from developing smooth muscle, which generates deep longitudinal epithelial folds that locally concentrate the Hh signal, promoting localized expression of cluster genes. By contrast, we show that in mouse, muscle-induced epithelial folding does not occur and artificial deformation of the epithelium does not determine the pattern of clusters or villi. In intestinal explants, modulation of Bmp signaling alters the spatial distribution of clusters and changes the pattern of emerging villi. Increasing Bmp signaling abolishes cluster formation, whereas inhibiting Bmp signaling leads to merged clusters. These dynamic changes in cluster pattern are faithfully simulated by a mathematical model of a Turing field in which an inhibitor of Bmp signaling acts as the Turing activator. *In vivo*, genetic interruption of Bmp signal reception in either epithelium or mesenchyme reveals that Bmp signaling in Hh-responsive mesenchymal cells controls cluster pattern. Thus, unlike in chick, the murine villus patterning system is independent of muscle-induced epithelial deformation. Rather, a complex cocktail of Bmps and Bmp signal modulators secreted from mesenchymal clusters determines the pattern of villi in a manner that mimics the spread of a self-organizing Turing field.

KEY WORDS: Villus formation, Epithelial-mesenchymal crosstalk, Mathematical model, Activator-inhibitor patterning model Turing field, Intestinal development, Morphogenesis

INTRODUCTION

The effective absorption of nutrients by the small intestine requires an enormous mucosal surface area. One adaptive mechanism for surface area amplification is the convolution of mucosal surface into a regular array of finger-like projections called villi. Villi arise at embryonic day (E) 14.5 in mice (week 8-10 in humans), when the intestine undergoes a remarkable morphogenic process to convert a pseudostratified epithelial tube surrounded by loose mesenchyme into a field of villi with mesenchymal cores, covered by columnar epithelium. Although the histological changes that accompany villus formation have been studied extensively (Dekaney et al., 1997; Dunn, 1967; Lacroix et al., 1984; Mathan et al., 1976; Matsumoto et al., 2002; Nakamura and Komuro, 1983; Sbarbati, 1982; Trahair and Robinson, 1986), the cellular and molecular drivers of this process are still incompletely understood, especially in mammals.

Recent progress has been made in deciphering the mode of villus emergence in the chick intestine. In that model, the initially flat epithelium gives way to longitudinal ridges, which evolve to regular zigzags and finally to villi, and these sequential morphological stages correlate with maturation of three smooth muscle layers (Coulombre and Coulombre, 1958; Shyer et al., 2013). The deep and regular folding of the epithelium, imposed by mechanical forces from the developing muscles, creates periodic maxima of epithelially secreted Hedgehog (Hh) protein beneath the folded epithelium that direct villus emergence in a regular manner (Shyer et al., 2015).

By contrast, in many mammals, including mouse (Sbarbati, 1982), rat (Dunn, 1967), sheep (Trahair and Robinson, 1986), pig (Dekaney et al., 1997) and human (Lacroix et al., 1984; Matsumoto et al., 2002), ridges and zigzags never form and in several of these systems (including mouse, as shown herein) villus formation is not temporally coordinated with smooth muscle development (de Castro, 2001; Fekete et al., 1996; Georgieva and Gerov, 1975; Kedinger et al., 1990; Keibel, 1910). Thus, localization of the Hh signal via smooth muscle-dependent epithelial deformation cannot explain the establishment of a uniform field of villi in many species; additional patterning forces are required.

In the mouse, villi arise as domes over condensed clusters of mesenchymal cells that express *Pdgfra* (Karlsson et al., 2000). We previously established that, prior to villus formation, scattered mesenchymal cells express *Gli1*, *Ptc1* (*Ptch1*) and *Pdgfra* (Karlsson et al., 2000; Walton et al., 2012). Hh ligands from the epithelium cause agglutination of these cells into clusters beginning at E14.5 (Walton et al., 2012). In mice overexpressing the pan-Hh inhibitor *Hhip*, clusters and villi fail to form (Madison et al., 2005). Similarly, in cultured intestinal explants inhibition of Hh signaling by cyclopamine or anti-Hh antibody (5E1) abolishes cluster formation and villus emergence, without altering smooth muscle (Fig. S1A,B,D,E) (Walton et al., 2012). By contrast, increasing the strength of the Hh signal increases cluster size, again without changing smooth muscle (Fig. S1C,F) (Walton et al., 2012), confirming that epithelial Hh controls a signaling cascade that drives mesenchymal cluster formation independently of alterations in the surrounding smooth muscle layers.

[1]Department of Cell and Developmental Biology, University of Michigan Medical School, Ann Arbor, MI 48109, USA. [2]Department of Molecular and Integrative Physiology, University of Michigan Medical School, Ann Arbor, MI 48105, USA. [3]Department of Biosciences and Nutrition, Karolinska Instituet, Novum, Huddinge SE-141 83, Sweden. [4]Department of Computational Medicine and Bioinformatics, University of Michigan Medical School, Ann Arbor, MI 48105, USA.

*Authors for correspondence (kdwalton@med.umich.edu; dgumucio@med.umich.edu)

Received 26 August 2015; Accepted 18 December 2015

Development (2016) 143, 427-436 doi:10.1242/dev.130112

Forming mesenchymal clusters are regularly positioned in the murine intestine, with an average cluster-to-cluster spacing of ~60-70 µm (Walton et al., 2012), suggesting that specific signals are required to generate such a well-patterned field. Although Hh signals control cluster agglutination and size, Shh and Ihh ligands are uniformly expressed by the pre-villus epithelium (Kolterud et al., 2009; Shyer et al., 2015); thus, it is unclear how epithelial Hh could establish the regular pattern of clusters, especially in species (e.g. mouse) in which there is no epithelial folding to create local Hh maxima. Since Bmp signaling is known to control a variety of patterning fields in other contexts (Hogan, 1996) and mesenchymal clusters in emerged villi express Bmp2 and Bmp4 (Karlsson et al., 2000), we examined the potential role of this pathway in cluster patterning.

Here, we show that newly established clusters express multiple Bmp ligands and Bmp signal modifiers. Moreover, abolishing Bmp signal reception changes cluster pattern, causing rows of mesenchymal cluster 'spots' to merge into 'stripes'. Merged clusters can also be generated by conditional deletion of Bmpr1a in Hh-responsive cells of the mesenchyme, whereas epithelial Bmpr1a deletion has no effect. This 'spots to stripes' pattern change is fully consistent with the mathematical predictions of a classical reaction-diffusion model, in which the overlapping activity domains of an activator and an inhibitor create a patterned field, as initially described by Turing (Maini, 2004; Meinhardt, 2012; Turing, 1952). In such a model, progressive saturation of the Turing activator (in this case posited to be a Bmp inhibitor) causes spots to become stripes. Together, our data establish that in the mouse model Bmp signaling controls cluster distribution. The patterning of clusters and emergence of villi in this model are not dependent upon muscular forces or epithelial deformation, but behave in accordance with a Bmp-dependent self-organizing Turing field.

RESULTS

Villus patterning in the mouse is not driven by tensile forces

Villus emergence correlates with smooth muscle development in chick (Coulombre and Coulombre, 1958; Shyer et al., 2013); thus, we examined whether this is also true in mouse. Such an analysis requires that the same region of the intestine (here, jejunum) be compared at all time points, since villus emergence propagates from proximal to distal intestine over a 24 h period (Walton et al., 2012). At E13.0, 48 h before villus morphogenesis initiates in the jejunum (Walton et al., 2012), a well-developed inner circular muscle (ICM) is already prominent (Fig. 1A) along the entire length of the intestine. A mature outer longitudinal muscle (OLM) is not seen until E16 (Fig. 1E), 24 h after the first villi emerge in the jejunum. Although a few scattered cells that are weakly positive for alpha smooth muscle actin (αSMA), a marker of mature smooth muscle, can be discerned at E15.0 (Fig. 1D), an organized OLM layer is absent at this time. Finally, the muscularis mucosa, which is immature at E16.5 (desmin positive, but αSMA negative; Fig. 1F), remains discontinuous at E18.5 (Fig. 1G). Thus, in the mouse, villus emergence is not temporally synchronized with the maturation of any of the three muscle layers.

Since formation of the ICM precedes villus development, we further examined whether confinement forces mediated by this muscle might play a role in cluster formation or villus emergence. E13.5 intestines (prior to cluster formation) were opened longitudinally, interrupting the circularity of the ICM (Fig. 1H). Although the ICM might still impose some force on the overlying tissue, radial confinement is abolished; indeed, opened intestines tend to invert. After 20 h in culture, clusters begin to form at the anterior end of the intestinal segment (Fig. 1I). By 38 h, clear, well-patterned mesenchymal clusters and rudimentary villi are visible (Fig. 1J,K). Villus and cluster size is uniform, even at the cut edges of the intestine, where residual strain is predicted to be lower (Fig. 1K, dashed line). Thus, in mouse, radial confinement from the ICM is not required for cluster formation, cluster patterning or initial villus emergence. We cannot, however, rule out the possibility that confinement from the ICM might facilitate the progression of villus outgrowth after initiation.

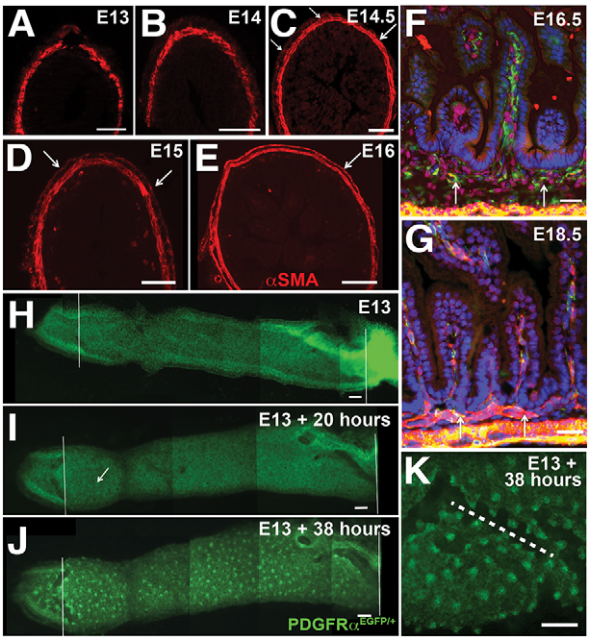

Fig. 1. Smooth muscle development does not correlate with mouse villus emergence; tensile forces are not required for cluster patterning. αSMA immunostaining (red) marks mature muscle cells in the developing muscle layers at E13 (A), E14 (B), E14.5 (C), E15 (D), E16 (E), E16.5 (F) and E18.5 (G). The ICM is already mature at E13 (A), but a mature OLM is not present until E16 (outer circle, arrow in E). Scattered αSMA$^+$ cells at E14.5 (arrows, C) and E15 (arrows, D) are not organized into a continuous muscle. (F,G) Muscularis mucosa is not present at E16.5 (F) and is still incomplete at E18.5 (G, arrows). Desmin (green) marks smooth muscle precursor cells (F, arrows). DAPI (blue) stains nuclei. (H-K) An E13 intestine from a *Pdgfra*$^{EGFP/+}$ mouse was opened longitudinally and cultured for 2 days. No clusters were present initially (H). Clusters began to develop by 20 h (I, near arrow). By 38 h, well-patterned clusters were visible (J) and small villi were emerging (magnified in K). The dashed line (K) indicates cut edges of the intestine, where it has rolled back after cutting. Clusters and villi were observed to form in intestines cut open prior to cluster formation and grown in culture for 2 days in more than 25 independent samples from at least eight separate experiments. Scale bars: 50 µm in A-G; 100 µm in H-K.

Epithelial deformation does not determine cluster pattern in the mouse intestine

In the chick, epithelial bending is an upstream driver of cluster formation and patterning. Thus, we examined the relationship between clusters and epithelial deformation in the mouse intestine. Thick (80-100 µm) vibratome sections of E14.5 mouse intestine were stained for α-tubulin, a marker that reveals epithelial cell shape and is also enriched in clusters, and confocal *z*-stacks were collected (Movie 1). Individual sections of the top, middle and bottom of a representative stack (Fig. 2A-C) reveal that the apical surface of the epithelium is still flat when the first clusters form basally beneath the epithelium. Thus, deep folds of the entire epithelium, such as those observed in the chick, are not seen in the mouse. On the basal

Development (2016) 143, 427-436 doi:10.1242/dev.130112

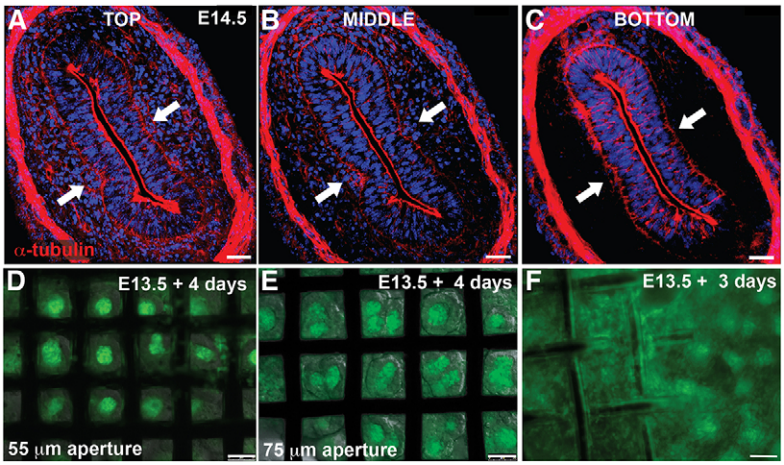

Fig. 2. Epithelial deformation does not determine cluster pattern in the mouse intestine. (A-C) Single slices from top (A), middle (B) and bottom (C) of a 50 µm thick *z*-section of an E14.5 intestine immunostained for α-tubulin (red) to outline epithelial cells and mark clusters (outer ring marks the ICM); DAPI (blue) marks nuclei. The arrows indicate the position of two clusters. Note basal epithelial deformation with no apical deformation. Movie 1 steps through the entire *z*-stack. (D-F) Mesh screens force deformation of the epithelium in E13.5 *Pdgfra*$^{EGFP/+}$ intestines that were cut open lengthwise and cultured under a mesh screen. (D) Individual villi with single mesenchymal clusters develop under a screen with a 55 µm aperture. (E) Multiple villi with a single cluster per villus develop under a mesh screen with a 75 µm aperture. (F) Note that cluster formation and villus development are delayed in tissue under a mesh screen (anterior, left side) as compared with the posterior side (right side) that was not under the screen. *n*>12 in four separate experiments for each of the mesh screen cultures. Scale bars: 30 µm in A-C; 50 µm in D-F.

side, however, epithelial cells directly above nascent clusters are shorter, creating shallow but obvious epithelial deformations (Fig. 2A-C, arrows). No basal deformations are detected in regions lacking a mesenchymal cluster or after treatment with cyclopamine (Fig. S1B) (Walton et al., 2012), which abolishes clusters, consistent with the idea that basal shortening is driven by signals from these clusters.

Although the analysis above suggests that cluster formation is upstream rather than downstream of basal epithelial deformation in the mouse, we tested directly whether artificially imposed epithelial deformation can drive cluster and villus pattern in this model. Shyer et al. (2015) deformed the chick intestinal epithelium by placing a grid on the opened epithelial surface and observed precocious induction of villus cluster genes and emergence of single villi through the holes of the grid. To take this analysis one step further, we utilized grids of different mesh sizes, placing them on the opened epithelial surface of the E13.5 mouse intestine, prior to cluster or villus formation. Intestinal explants were observed daily for 4 days. We reasoned that, if epithelial deformation is a critical determinant of cluster and villus pattern in the mouse, grids of increasingly wider mesh size should produce increasingly wider clusters and villi. However, this was not seen (Fig. 2D-F). Mesh sizes that approximate cluster size (55 µm aperture) allowed single villi to grow into the mesh spaces (Fig. 2D), as seen previously (Shyer et al., 2015). However, in grids with larger mesh sizes (75 µm aperture and larger), multiple clusters (and villi), rather than larger clusters and villi, were observed (Fig. 2E). Additionally, analysis of the boundary of the grid revealed that grid placement slowed rather than accelerated cluster formation and villus emergence (Fig. 2F). Together, these experiments demonstrate that, for the mouse intestine, epithelial deformation is not sufficient to impart patterning cues to the field of clusters and emerging villi. Rather, the presence and patterning of mesenchymal clusters determines the presence and pattern of the emerging villi. We therefore sought to identify the signal(s) downstream from Hh-mediated cluster aggregation that is responsible for cluster patterning.

Mesenchymal clusters express multiple Bmp signaling molecules

Bmps are secreted ligands responsible for patterning in many developmental contexts (Hogan, 1996), and several Bmp ligands are known targets of Hh signaling (Roberts et al., 1995). To better assess the potential involvement of Bmp signaling during cluster formation and patterning of nascent clusters, we examined the localization of RNA transcripts for several Bmp ligands and modifiers during the initial round of cluster formation as well as in clusters associated with emerged villi (Fig. 3). Prior to cluster formation, *Bmp4*, *Bmp5* and *Bmp7* are expressed in many cells of the subepithelial mesenchyme, whereas *Bmp2* is primarily epithelial (Fig. 3A-D). As clusters form (E14.5), *Bmp2* expression is initiated in clustered cells (Fig. 3A, inset). As villi emerge (E15.5), all Bmp genes except *Bmp7* are expressed robustly in mesenchymal clusters (Fig. 3I-L); *Bmp2* continues to be the most specific cluster marker (Fig. 3I). The expression pattern of the Bmp modifier twisted gastrulation 1 (*Twsg1*) (Fig. 3E,M) is similar to that of *Bmp5*, while the tolloid-like molecule *Bmp1* is weakly expressed at E14.5 (Fig. 3F) but is high in mesenchymal clusters at E15.5 (Fig. 3N). The Bmp inhibitor noggin (*Nog*) is expressed in mesenchymal

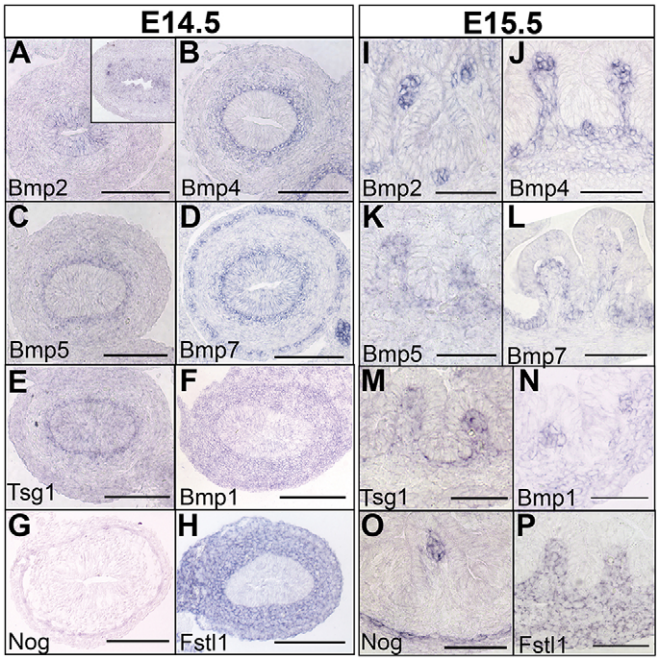

Fig. 3. RNA *in situ* hybridization of Bmp pathway ligands and modifiers. Analysis was performed at E14.5 just prior to cluster formation and villus emergence (A-H), and at E15.5 once villi have begun to emerge (I-P). The inset (A) shows cluster-specific expression of *Bmp2* in nascent clusters at a slightly later stage, when expression is switching from epithelial to mesenchymal. Scale bars: 100 µm.

Development (2016) 143, 427-436 doi:10.1242/dev.130112

clusters only after emergence (Fig. 3G,O), whereas follistatin-like 1 (*Fstl1*) is highly expressed throughout the mesenchyme at both stages (Fig. 3H,P). Thus, multiple Bmp ligands and Bmp signaling modifiers are dynamically expressed both in unclustered mesenchyme and in nascent and mature mesenchymal clusters.

Modulation of Bmp signaling affects cluster formation and pattern

To determine whether Bmp ligands or signaling modifiers could modulate cluster pattern, intestines from E13.5 $Ptc^{lacZ/+}$ embryos (prior to cluster formation) were cultured on transwell filters in the presence of agarose beads soaked in bovine serum albumin (BSA, control) or recombinant Bmp2, Bmp4, Bmp5, Bmp7, or heterodimerized Bmp2/7 or Bmp4/7. After 2 days, clusters formed in the expected pattern near control beads (Fig. 4A,D,G,J). However, all Bmp-soaked beads inhibited mesenchymal cluster formation and subsequent villus emergence in the region surrounding the bead, but not on the opposite side of the intestine (Fig. 4B,C,E,F,H,I,K, Fig. S2). Lack of cluster formation near Bmp beads was confirmed by immunostaining for Pdgfrα, a marker of mesenchymal clusters (Karlsson et al., 2000) (Fig. 4K). Bmp2 was the most potent ligand for inhibiting cluster formation near the beads, strongly inhibiting cluster formation at 125 ng/ml and above (Fig. 4L, Fig. S2E).

Similarly, we tested the effects of several of the Bmp signaling modulators that are expressed in clusters (Fig. 5). The cluster patterning perturbations were more subtle, consisting of larger or merged clusters rather than a clearing of clusters (Fig. 5A-C). Pattern changes for Twsg1 were most obvious (Fig. 5C), although cluster sizes for intestines treated with Bmp1, Nog or Twsg1 in the medium (10 ng/ml) were all statistically different from clusters treated with BSA (Fig. 5E). Clusters closest to Twsg1-soaked beads (250 ng/ml) placed on top of the intestine were significantly larger than clusters more distant from the bead (Fig. 5D). Clusters in BSA-treated intestines did not differ in size from clusters distant from Twsg1 beads (Fig. 5E).

Next, we tested the effect of complete Bmp signal inhibition on cluster formation and villus emergence. Intestines were harvested prior to cluster formation and cultured for 2 days with a small-molecule inhibitor of Bmp signaling, dorsomorphin (Fig. 6). Inhibition of Bmp signaling in this manner alters cluster patterning dramatically. Clusters are two to three times larger and often connected, so that the 'spot-like' distribution of clusters in control intestines (Fig. 6A-C) becomes 'striped' in the presence of dorsomorphin (Fig. 6D-F). In transverse sections of the intestines, the larger merged clusters are seen to alter the shapes of associated villi (compare Fig. 6G-J). These changes occur without altering smooth muscle (Fig. 6H-L), again confirming that cluster pattern, not muscle tension, determines the pattern of villus emergence in the mouse.

Studies in other systems have shown that inhibition of Bmp signaling in the epithelium causes cells to shorten and become columnar or cuboidal (Eom et al., 2011; Gibson and Perrimon, 2005; Rajagopal et al., 2009; Shen and Dahmann, 2005). However, dorsomorphin treatment does not cause widespread columnar conversion; epithelium above the merged clusters is columnar, while epithelium between these clusters remains pseudostratified (Fig. 6M-O). Doubling the dose of dorsomorphin generates larger clusters and larger villi, but does not convert all epithelial cells to a columnar shape (Fig. 6O). Thus, inhibition of Bmp signaling throughout the intestine affects cluster pattern without altering cell shape in the epithelium.

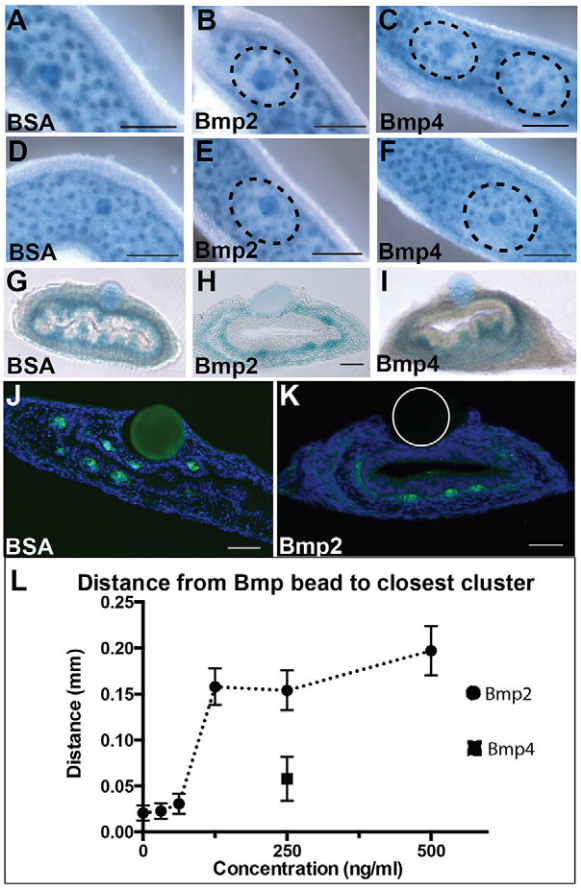

Fig. 4. Bmp ligand-soaked agarose beads inhibit cluster formation and villus emergence. (A-I) E13.5 $Ptc^{lacZ/+}$ intestines were harvested prior to cluster formation and cultured for 2 days with agarose beads soaked in BSA or recombinant protein, as indicated. X-gal staining shows the pattern of $Ptc^{lacZ/+}$ clusters that form in whole (A-F) or transverse sectioned (G-I) intestines. Hatched ovals (B,C,E,F) outline the clearance of $Ptc^{lacZ/+}$ clusters around the Bmp-soaked bead; faint clusters that appear within the hatched oval are on the transwell/opposite side of the intestine, as seen in the transverse sections in H and I. (J,K) Pdgfrα immunostaining (green) marks clusters formed near a BSA-soaked bead (J), which are absent around the Bmp-soaked bead (K). Inhibition of cluster formation near Bmp-soaked beads was observed in at least 100 beads placed on more than 25 intestines. (L) Scatterplot of the mean of the distances from the edge of Bmp2-soaked beads or Bmp4-soaked beads to the nearest clusters measured in a sampling from those experiments (at least six beads placed on at least three different intestines). Error bars are s.d. See also Fig. S2 for measurements of clearing around other Bmp ligand-soaked beads. Scale bars: 50 µm.

We previously showed that increased Hh signaling also produces larger clusters (Walton et al., 2012), although a striped pattern was not seen. Here, dorsomorphin treatment does not appear to dramatically affect the expression levels of the Hh target gene *Ptc1* in these $Ptc1^{lacZ/+}$ intestines. Lack of a significant effect of dorsomorphin on the Hh signaling pathway was further confirmed by qRT-PCR (Fig. S3).

Genetic loss of Bmpr1a in mesenchymal clusters impacts cluster size and villus morphology

Although the experiments above reveal the importance of Bmp signaling in modulating cluster pattern, they do not establish which compartment (epithelial, mesenchymal or both) must transduce Bmp signals to control this process. Since Bmp signaling activity is detected in both the epithelium and mesenchyme (Fig. S4), we used

Development (2016) 143, 427-436 doi:10.1242/dev.130112

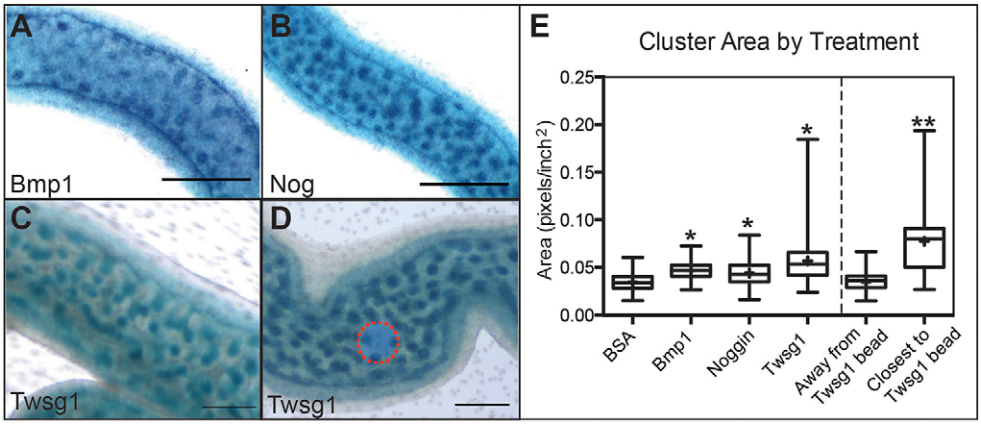

Fig. 5. Bmp modifiers alter cluster pattern and villus shape. E13.5 $Ptc^{lacZ/+}$ intestines were harvested prior to cluster formation and cultured for 2 days with 10 ng/ml recombinant protein as indicated (A-C) or 250 ng/ml Twsg1 on agarose beads (D, hatched circle). (A-D) X-gal staining shows the pattern of $Ptc^{lacZ/+}$ clusters that form in whole intestines. Note that the merging of clusters is most dramatic in Twsg1-treated intestines in C and near the Twsg1 beads in D. (E) Box and whisker plot of cluster areas showing the largest, smallest, median (center line) and mean (+) for each treatment. Cluster areas for Bmp1-treated and Nog-treated intestines were significantly different from those of BSA-treated and Twsg1-treated intestines (*P<0.0001), but were not different from each other. Twsg1-treated intestines were significantly different from BSA-treated intestines (*P<0.0001). Clusters immediately surrounding Twsg1-soaked beads were significantly different in size from clusters at a distance from the beads (**P<0.0001), but not from clusters in BSA-treated intestines (P=0.689). Scale bars: 250 µm in A,B; 100 µm in C,D.

a conditional $Bmpr1a^{f/f}$ mouse model (Mishina et al., 2002), in combination with tissue-specific Cre drivers, to genetically delete Bmpr1a signaling in either the mesenchyme (using $Gli1^{CreERT2/+}$) (Bai et al., 2002) or the epithelium (with Shh^{Cre}) (Harfe et al., 2004) prior to cluster formation. Demonstration of reporter expression and qRT-PCR showing the efficacy of deletion are shown in Fig. S5.

Loss of *Bmpr1a* in the epithelium (Shh^{Cre}; activated by E9.5) (Harfe et al., 2004) does not affect muscle development, cluster size, cluster distribution or epithelial morphology (Fig. 7A,B). However, loss of Bmpr1a in Hh-responsive mesenchymal cells results in larger clusters and wide villi (Fig. 7C,D), a phenotype closely resembling that seen in intestines treated with dorsomorphin. Scanning electron microscopy (SEM) confirms larger/merged villi in the $Bmpr1a^{f/f}$; $Gli1^{CreER/+}$ mutants as compared with control littermates (Fig. S6). Indeed proliferation was increased with loss of Bmpr1a in the mesenchyme; however, neither the amount (Fig. S7) nor the pattern of proliferation (Fig. S8) was altered in the epithelium. Together, these data demonstrate that the patterning of mesenchymal clusters is determined by the level of Bmp signal transduction in the Hh-responsive mesenchymal compartment.

Cluster patterning resembles a spreading Turing field

We previously showed that mesenchymal clusters are established in an anterior to posterior and dorsal to ventral wave, eventually generating a regular pattern along the length of the intestine (Walton et al., 2012). Turing first postulated that similar patterns can be generated by the reactions of diffusive chemicals; small perturbations in initially uniformly distributed chemicals can increase in amplitude over time, leading to a regular spatial pattern. The Turing system employs an activator and an inhibitor, both expressed by the same cell or group of cells. The inhibitor spreads further than the activator, and patterned spots become stripes when the activator is saturating (Turing, 1952).

Cluster patterning *in vivo* shares several features with the Turing system. (1) An initially homogeneous state, lacking clusters and villi, evolves quickly (within 12 h) to a patterned state that then spreads (Walton et al., 2012). (2) The pattern can be altered by Bmp ligands, which inhibit the formation of clusters where Bmp signaling is high (Fig. 4, Fig. S2); thus, one or more Bmp ligands may act as Turing inhibitors. (3) Dorsomorphin treatment changes the cluster pattern from spots to stripes (Fig. 6) and beads soaked with several Bmp inhibitors/modulators cause cluster fusion into short stripes (Fig. 5), suggesting that an inhibitor of Bmp signaling could be the Turing activator. (4) Multiple Bmp ligands and signaling modulators are expressed by cluster cells (Fig. 3), in accordance with the requirement for expression of activator and inhibitor by the same cells. (5) The genetic experiments above show that patterning requires the reception of Bmp signals in the mesenchymal compartment, including the cluster cells themselves (Fig. 7).

To test the degree to which a mathematical model of a Turing system resembles the experimentally derived data, we constructed a Turing system comprising two modulators of Bmp signaling following a ‘pure activator-inhibitor’ system (Dillon and Othmer, 1993) and incorporating cell density (see the supplementary Materials and Methods for details). We propose that the Turing activator is a Bmp inhibitor and that the Turing inhibitor consists of one or more Bmp ligands. The evolution of the resulting pattern, represented as cell density, in the absence or presence of saturating activator (Bmp inhibition/dorsomorphin) is displayed in Fig. 8A,B. Light-green regions represent high concentrations of Bmp inhibitor (Turing activator), while the dark regions represent low concentrations. In our model, mesenchymal cluster cells are assumed to produce these proteins, whose interactions give rise to these gradients, so that regions of high Bmp inhibitor correspond to the location of mesenchymal cells where clustering occurs. As predicted by the Turing system, spots are seen when the activator concentration is well below saturation, whereas saturation of the activator produces larger clusters and areas with a stripy pattern. These patterns closely resemble those observed experimentally, including the 2- to 3-fold increase in cluster size with saturating activator (Bmp inhibitor) (plotted in Fig. 8M,N).

We then used the model to predict the patterns that would evolve with intermediate levels of activator. At such intermediate levels, spots and stripes were mixed and stripes were predicted to be shorter and less frequent (Fig. 8C). This was indeed borne out

Development (2016) 143, 427-436 doi:10.1242/dev.130112

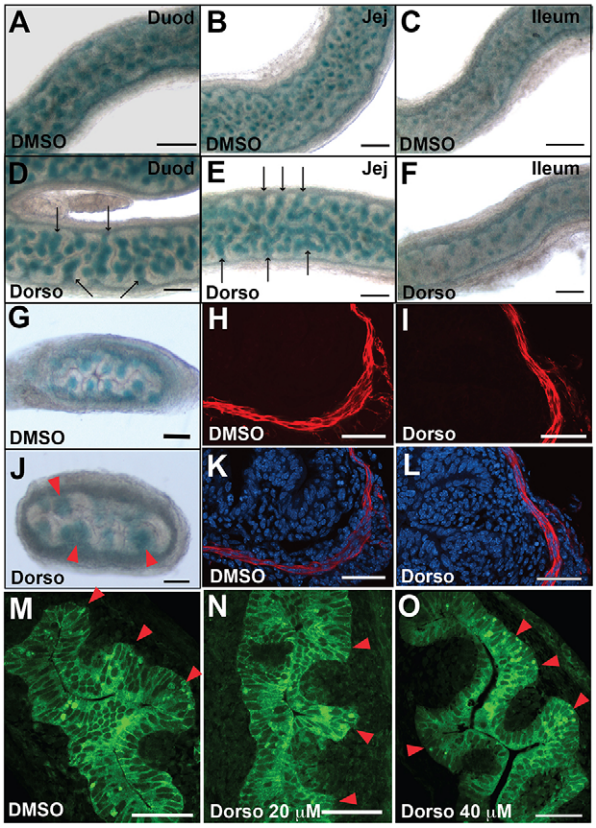

Fig. 6. Inhibition of Bmp signaling alters cluster pattern and villus size. *Ptc*$^{lacZ/+}$ intestinal pieces were harvested at E13.5 and cultured with DMSO (A-C,G,H,K,M), 20 µM dorsomorphin (D-F,I,J,L,N) or 40 µM dorsomorphin (O). Treatments were performed in at least 25 control and 35 dorsomorphin-treated intestines; representative images of duodenum (A,D), jejunum (B,E,G-O) and ileum (C,F) are shown. After 2 days, intestines were fixed and X-gal stained to show the pattern of *Ptc*$^{lacZ/+}$ clusters (blue) in whole intestines (A-F) and 100 µm sections (G,J). Arrows in D,E mark areas where clusters merge to stripes with dorsomorphin treatment. Arrowheads in J mark large fused clusters and large villi. (H,I,K,L) Dorsomorphin treatment does not alter smooth muscle (αSMA, red). Sections are shown with (K,L) and without (H,I) DAPI staining. (M-O) Epithelial cells (outlined by E-cadherin immunostaining, green) remain pseudostratified in intervillus regions (red arrowheads) when Bmp signaling is inhibited (N,O), similar to controls (M). Scale bars: 100 µm in A-F; 50 µm in G-O.

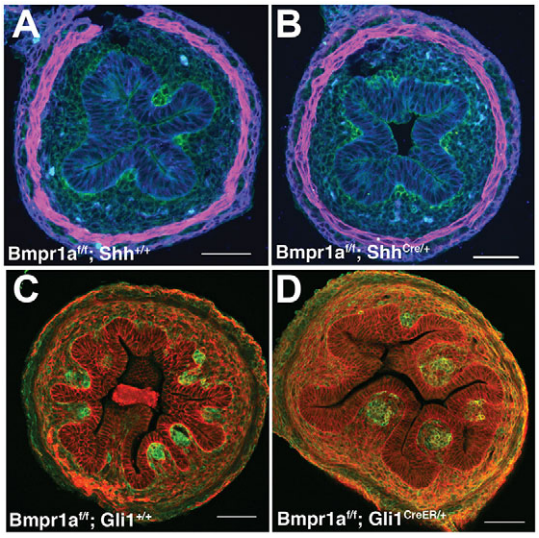

Fig. 7. Conditional loss of Bmp signaling in Hh-responsive mesenchymal cells, but not in epithelial cells, results in fused clusters and wide villi. (A,B) *Bmpr1a*$^{f/f}$ mice were mated to *Shh*^{Cre} mice. *Shh*^{Cre} is activated by E10 in the intestinal epithelium (Kolterud et al., 2009). No changes in epithelial (E-cadherin, blue) or mesenchymal pattern (Pdgfrα, green) were noted; muscle was unchanged (αSMA, magenta). (C,D) *Bmpr1a*$^{f/f}$ mice were mated with *Gli1*$^{CreERT2/+}$ mice. Recombination was induced with three doses of tamoxifen, beginning at E12.5 prior to cluster formation, and tissues were harvested at E15.5. Large clusters (Pdgfrα, green) and wide villi (E-cadherin, red) are seen in *Bmpr1a*$^{f/f}$; *Gli1*^{CreER} mutant intestines (D). Eight mutant and eight control littermate intestines from three separate litters were analyzed for *Bmpr1a*$^{f/f}$; *Shh*^{Cre}. Twenty mutant and 21 control littermate intestines from six separate litters were analyzed for *Bmpr1a*$^{f/f}$; *Gli1*^{CreER}. Scale bars: 50 µm.

experimentally, after exposure of intestinal explants to an intermediate dose of dorsomorphin (Fig. 8G). We also modeled a localized source of high concentration of Turing inhibitor (Bmp ligand) and found that the resulting simulation (Fig. 8D) mirrored our experimental results of intestines cultured with Bmp ligand-soaked agarose beads (Fig. 4, Fig. 8H, Fig. S2E). Finally, we examined a scenario in which a spot-like pattern was allowed to evolve for 24 h in the absence of saturated activator, and then activator concentration was computationally increased in a stepwise fashion. In this simulation, the initial spot-like pattern evolved to become more stripe-like (Fig. 8I,J, Movie 2). Experimentally, we allowed E13.5 intestines to develop for 48 h on transwells, until the spot-like pattern of clusters became apparent (Fig. 8K) and then added dorsomorphin to the culture for an additional 48 h. The initial spot pattern filled in to become stripy, in a manner closely resembling the computed simulation (Fig. 8L). Overall, these results provide strong evidence that cluster patterning and subsequent villus emergence are controlled, at least in part, by Bmp signaling and that the patterning field evolves in a manner consistent with a self-organizing Turing field within the mesenchyme.

DISCUSSION

Optimal absorptive function by the small intestine depends upon the generation of a tightly packed and well-organized field of villi, a process that begins in fetal life. Substantial evidence over the past several decades has emphasized the role of complex epithelial-mesenchymal crosstalk in the process of villus formation [for a recent review, see Wells and Spence (2014)]. Indeed, we previously established that one of the earliest steps in villus development takes place at E14.5 in the mouse, when Hh signals, expressed uniformly from the epithelium (Kolterud et al., 2009), act on evenly distributed *Ptc1*$^{+}$ *Gli1*$^{+}$ *Pdgfra*$^{+}$ subepithelial mesenchymal cells, causing their aggregation into mesenchymal clusters (Walton et al., 2012). Here, we provide evidence that, downstream from this cluster-forming epithelial Hh signal, a Bmp signaling network that operates entirely within the mesenchyme is responsible for establishment of cluster spacing and pattern. We show that cluster pattern can be dynamically altered simply by modifying the concentration of Bmp ligands or Bmp signaling modifiers and that the pattern evolves in a manner consistent with a Turing activator/inhibitor field.

There is mounting evidence for the validity of Turing-based models to explain pattern evolution in several diverse biological systems, including feather bud arrangements (Baker et al., 2009), hair follicle spacing (Maini et al., 2006; Sick et al., 2006), palatal rugae distribution (Economou et al., 2012), tongue papilla patterning (Zhou et al., 2006), digit patterning (Raspopovic et al., 2014) and zebrafish mesodermal pigmentation (Eom et al., 2012; Kondo and Miura, 2010), and it is interesting that Bmp ligands

Development (2016) 143, 427-436 doi:10.1242/dev.130112

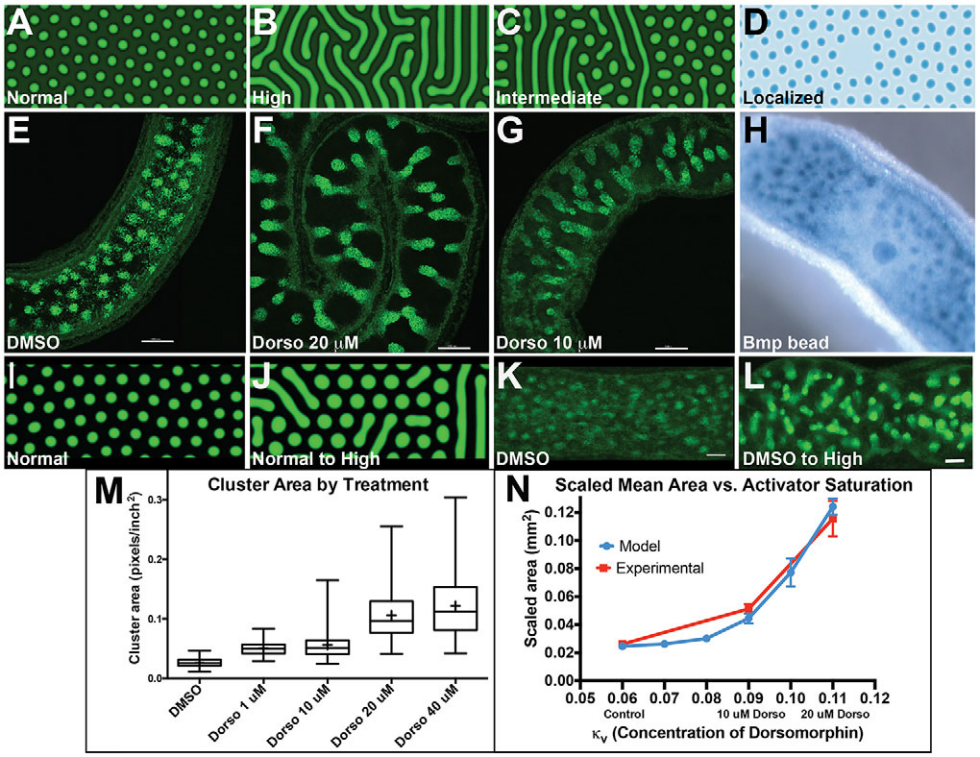

Fig. 8. A Turing field model of cluster cell patterning recapitulates the experimental data. (A-D) Still images of the patterns predicted by the simulations (further details are provided in the supplementary Materials and Methods). A regularly spaced pattern of clusters (spots) is predicted in control (A) Turing simulations. The pattern is altered to stripes (B) when the Turing activator (Bmp inhibitor) is saturated. An intermediate level of activator results in shorter stripes (C, lower dose of dorsomorphin), while a localized increase in Turing inhibitor (excess Bmp ligand at center) prevents cluster formation near the source (D). (E-H) Representative images of experimental results obtained under treatment conditions that match the Turing simulations. Treatments were as follows: control (E), 20 μM dorsomorphin (F), 10 μM dorsomorphin (G) and Bmp-soaked bead (250 ng/μl) (H). (I-L) Dynamic changes in Bmp inhibitor concentration change patterns in simulations and experimental tests. A developed spot pattern (I) evolved toward stripes (J) when the inhibitor concentration was computationally increased. Experimentally, established cluster spots (K) merge to form short stripes (L) when dorsomorphin (20 μM) is added (n=18 intestines). Scale bars: 100 μm. (M) Box and whisker plot showing the largest, smallest, median (middle line) and mean (+) cluster area for intestines treated for 2 days with vehicle (DMSO) or increasing doses of dorsomorphin. n=5 fields for at least five different intestines for DMSO, 10 μM, 20 μM, 40 μM dorsomorphin; n=5 fields for three different intestines for 1 μM dorsomorphin. (N) Scatter plot comparing the average cluster area at increasing concentrations of dorsomorphin (experimental) verses the simulated model. Error bars are s.e. The s.d. increases with increasing concentrations of Bmp inhibitor due to striped patterns and boundary conditions (n=73, 75, 74, 34, 15, 3 for the increasing concentrations of dorsomorphin).

appear to act as Turing inhibitors in several of these systems (Garfinkel et al., 2004; Harris et al., 2005; Mou et al., 2011). In the intestine, we have seen that several different Bmp ligands are expressed by clusters (Bmp2, 4, 5, 7) and functional assays indicate that high concentrations of all of these Bmps act to inhibit the formation of clusters (Fig. 4, Fig. S2). Similarly, multiple Bmp signaling modifiers are expressed by clusters (Nog, Twsg1, Bmp1, Fstl1) and several of these cause pattern perturbations in the explant agarose bead assay (Fig. 5). Thus, although we show that pattern formation in the intestine is faithfully modeled by a computational framework that embodies a two-component system, as originally described by Turing (1952), it is highly likely that pattern establishment and maintenance *in vivo* are actually a product of a much more complex combination of Bmp pathway components. In fact, in the introduction to his classical paper describing such patterning fields, Turing himself stated that his model is an idealization and simplification of reality (Turing, 1952).

In addition to their role in patterning, our data suggest that signals from mesenchymal clusters are responsible for the epithelial cell shape changes that initiate villus emergence. Epithelial cells begin to shorten apicobasally as clusters first form (Fig. 2). If clusters do not form [for example, after inhibition of Hh signaling (Madison et al., 2005; Walton et al., 2012) or in the vicinity of a Bmp-soaked bead], the epithelium remains pseudostratified. By contrast, induction of larger clusters [e.g. smoothened agonist (SAG; a synthetic Hh pathway agonist that binds smoothened) or dorsomorphin treatment] results in larger villi, over which more epithelial cells take on a columnar shape (Walton et al., 2012). Since, in the fly wing disc, clonal loss of the Bmp receptor *thickveins* causes cells to become columnar (Gibson and Perrimon, 2005), we predicted that epithelial Bmpr1a deletion or addition of dorsomorphin to cultured intestines would cause widespread conversion to epithelial columnar morphology. This was not observed. Thus, our studies suggest that Bmp signaling alone does not mediate the epithelial cell shape changes that occur over villus clusters. Determining the pathway(s) responsible for this morphogenic process, which is likely to provide an important part of the driving mechanism for villus outgrowth, remains an important future goal.

It is interesting that, although the use of intestinal villi to expand intestinal surface area is a well-conserved attribute in multiple species, divergent strategies for patterning of the villi have emerged during evolution. In the chick intestine, recent studies have shown that tensile forces from developing smooth muscles progressively deform the epithelium to create localized peaks of Hh protein underneath sharply bent epithelial alcoves; these Hh maxima seem to determine the location of the villi (Shyer et al., 2015). However,

Development (2016) 143, 427-436 doi:10.1242/dev.130112

our data show that a different epistatic relationship between cluster formation, muscular forces and epithelial deformation portends in the mouse. Maturation of the various smooth muscle layers does not correspond temporally with the process of villus emergence in the murine intestine. Additionally, the epithelium is not remodeled into ridges or zigzags prior to villus formation; rather, villi arise as discrete domes directly from a flat epithelial surface. Although we did note soft basal epithelial deformations above nascent clusters, previous modeling studies suggest that such minimal bending is unlikely to create a substantial concentration of Hh signals (Shyer et al., 2015). Moreover, we never observed these soft basal deformations in the absence of a cluster; indeed, our evidence suggests that the deformations are a consequence of unknown signals from the underlying clusters. We provide extensive evidence that mesenchymal clusters and Bmp signaling in cluster cells control villus pattern in the mouse. Directly perturbing mesenchymal cluster pattern by altering Bmp signaling does not affect smooth muscle development (Figs 6 and 7) but does alter the pattern of clusters, thereby producing predictable changes in the pattern of the villi (Fig. 8). In fact, dramatic changes in Bmp concentration can even alter established patterns (Fig. 8I-L). Strikingly, however, despite the different modes of villification in the chick and mouse, conserved signaling pathways are involved: Hh signals from the epithelium play central roles in the induction of cluster genes, such as Bmp, in both species.

As in mouse, the intestines of human, pig and rat lack the zigzag-like structures of chick intestine (Dekaney et al., 1997; Lacroix et al., 1984; Matsumoto et al., 2002; Nakamura and Komuro, 1983). Although the proximal human intestine may contain short ridge-like structures that are later broken up into individual villi (Johnson, 1910), the human distal small intestine develops villi directly, as in the mouse (Johnson, 1910). Additionally, only the ICM, which may play a confinement role, aiding but not initiating villus emergence, is formed prior to villus emergence, and maturation of the remaining smooth muscle layers in the human (Fekete et al., 1996; Keibel, 1910), pig (de Castro, 2001; Georgieva and Gerov, 1975) and rat (Kedinger et al., 1990) occurs well after the initiation of villus formation, as in mouse. It is therefore likely that these mammalian species also rely on a villification patterning process that is controlled by gradient fields of signaling proteins rather than employing the avian model of muscle-directed epithelial deformation. It is also important to note that several rounds of villus formation have been demonstrated in the mouse (Walton et al., 2012) and are likely to occur in all species. Once the initial pattern is set, a Turing-like patterning mechanism in a growing domain could act to establish the arrangement of subsequent mesenchymal clusters, thereby generating a field of uniformly patterned villi in the intestine of all these species, including chick.

MATERIALS AND METHODS

Mice

Mice were handled humanely according to UCUCA guidelines. The following lines were used: C57BL/6 and CD1 (Charles River); *Rosa*$^{mT/mG}$ (Muzumdar et al., 2007), *Pdgfra*$^{EGFP/+}$ (Hamilton et al., 2003), *ShhEGFP*$^{Cre/+}$ (Harfe et al., 2004), *Ptc*^{lacZ} (Goodrich et al., 1997), *Gli1*^{CreERT2} (Bai et al., 2002) (all Jackson Labs); and *Bmpr1a*$^{f/f}$ (Mishina et al., 2002) (Dr Yuji Mishina).

Tamoxifen induction of recombination

Pregnant females were gavage fed daily from E12.5-14.5 with 250 µl 20 mg/ml tamoxifen dissolved in corn oil. Embryos were collected at E15.5.

Cultures, recombinant proteins and inhibitors

Embryonic intestines were harvested at E12.5 or E13.5 and grown in culture with protein-soaked agarose beads or dorsomorphin as described (Walton and Kolterud, 2014). Media were changed twice daily. Bmp2, Bmp4, Bmp5, Bmp7, Nog, Bmp1, Twsg1, and heterodimerized Bmp2/7 and 4/7 recombinant proteins were obtained from R&D Systems.

Cluster area measurements

Using ImageJ software (NIH), ellipses were drawn around clusters to measure area. All statistical tests were performed in Excel (Microsoft) or Prism (GraphPad). Unless otherwise noted, *t*-tests were two-tailed and non-parametric.

Mesh screen cultures

E13.5 intestines were harvested from *Pdgfra*$^{EGFP/+}$ embryos, cut open lengthwise and placed on a transwell membrane to expose the luminal surface. Mesh screens (55 or 75 µm, the Mesh Company, #300 or #230) were cut to size and placed on top of the intestines to culture for 1 week, with images acquired daily.

Tissue fixation and immunostaining

Epithelial-mesenchymal separation is described in the supplementary Materials and Methods. Tissues were fixed for 2 h at room temperature or overnight at 4°C in 4% paraformaldehyde. Vibratome, paraffin, and frozen sections were prepared as previously described (Walton and Kolterud, 2014; Walton et al., 2012). Antibodies used were: Pdgfrα (Santa Cruz, sc338; 1:200), E-cadherin (BD Biosciences, 610181; 1:1000), αSMA (Sigma, C6198; 1:500), desmin (Abcam, ab8592; 1:500), ezrin (Sigma, E8897; 1:500), α-tubulin (Sigma, T6199; 1:1000). Additional antibodies used were Ki67 (NovaCastra, L111859; 1:750), BrdU (Accurate, OBT0030G; 1:200) and CD44v6 (eBiosciences, BMS145; 1:1000) followed by tyramide signal amplification with the Molecular Probes T20932 Kit. BrdU immunostaining to determine proliferation index is described in the supplementary Materials and Methods.

Scanning electron microscopy (SEM)

Tissues were prepared for SEM as described in the supplementary Materials and Methods and the luminal structure was imaged on an AMRAY 1910 field emission scanning electron microscope.

RNA *in situ* hybridization

RNA *in situ* hybridization was performed on 8 µm frozen sections as described previously (Li et al., 2007).

Quantitative RT-PCR

Purified RNA was reverse transcribed and then subjected to qRT-PCR as described in the supplementary Materials and Methods using the primers listed in Table S1.

Turing field simulations

In our model, the activator-inhibitor interactions assume a saturating source of both the activator species (u) and the inhibitor species (v), the latter of which is altered by pharmacological inhibitors of Bmp signaling such as dorsomorphin (Gierer and Meinhard, 1972). The saturating source of u is also inhibited by the presence of v, according to the classic Turing activator-inhibitor system. We include density-dependent cell proliferation, along with the diffusive and chemotactic movement of the mesenchymal cells. Additional details of the Turing model are provided in the supplementary Materials and Methods.

Acknowledgements

We gratefully acknowledge mouse lines shared by Dr Yuji Mishina and Dr Alexandra Joyner. We thank University of Michigan colleagues for helpful discussions and advice: Drs Yuji Mishina, Doug Engel, Jason Spence, Ben Allen, Deneen Wellik and Linda Samuelson. We are grateful to Dr Cliff Tabin for providing unpublished data on chick villus patterning and for stimulating discussions on villus patterning.

Competing interests
The authors declare no competing or financial interests.

Author contributions
K.D.W., M.W., S.K.S., A.K., S.S. and D.L.G. contributed to concepts and approaches; K.D.W., A.K., M.J.C., J.K., N.P., D.C. and A.M.F. performed experiments; K.D.W., M.W., S.K.S., A.K., S.S. and D.L.G. analyzed data; K.D.W. and D.L.G. prepared the manuscript; K.D.W., S.K.S., A.K., S.S. and D.L.G. edited the manuscript.

Funding
Support was provided by National Institutes of Health (NIH) grants [R01 DK065850 and R01 DK089933 to D.L.G.] and an NIH Institutional Research and Academic Career Development Award Fellowship (to M.W.). Deposited in PMC for release after 12 months.

Supplementary information
Supplementary information available online at
http://dev.biologists.org/lookup/suppl/doi:10.1242/dev.130112/-/DC1

References

Bai, C. B., Auerbach, W., Lee, J. S., Stephen, D. and Joyner, A. L. (2002). Gli2, but not Gli1, is required for initial Shh signaling and ectopic activation of the Shh pathway. *Development* **129**, 4753-4761.
Baker, R. E., Schnell, S. and Maini, P. K. (2009). Waves and patterning in developmental biology: vertebrate segmentation and feather bud formation as case studies. *Int. J. Dev. Biol.* **53**, 783-794.
Coulombre, A. J. and Coulombre, J. L. (1958). Intestinal development. I. Morphogenesis of the villi and musculature. *J. Embryol. Exp. Morphol.* **6**, 403-411.
de Castro, A. M. M. G., Alvares, E. P., Zocoller-Seno, M. C., Neves, M. F. and Passipieri, M. (2001). Morphological study of the small intestine of moura pigs (Sus scrofa- Lineaus, 1758) during fetal development. *Braz. J. Morphol. Sci.* **18**, 95-101.
Dekaney, C. M., Bazer, F. W. and Jaeger, L. A. (1997). Mucosal morphogenesis and cytodifferentiation in fetal porcine small intestine. *Anat. Rec.* **249**, 517-523.
Dillon, R. and Othmer, H. G. (1993). Control of gap junction permeability can control pattern formation in limb development. *Exp. Theor. Adv. Biol. Pattern Format.* **259**, 65-81.
Dunn, J. S. (1967). The fine structure of the absorptive epithelial cells of the developing small intestine of the rat. *J. Anat.* **101**, 57-68.
Economou, A. D., Ohazama, A., Porntaveetus, T., Sharpe, P. T., Kondo, S., Basson, M. A., Gritli-Linde, A., Cobourne, M. T. and Green, J. B. (2012). Periodic stripe formation by a Turing mechanism operating at growth zones in the mammalian palate. *Nat. Genet.* **44**, 348-351.
Eom, D. S., Amarnath, S., Fogel, J. L. and Agarwala, S. (2011). Bone morphogenetic proteins regulate neural tube closure by interacting with the apicobasal polarity pathway. *Development* **138**, 3179-3188.
Eom, D. S., Inoue, S., Patterson, L. B., Gordon, T. N., Slingwine, R., Kondo, S., Watanabe, M. and Parichy, D. M. (2012). Melanophore migration and survival during zebrafish adult pigment stripe development require the immunoglobulin superfamily adhesion molecule Igsf11. *PLoS Genet.* **8**, e1002899.
Fekete, E., Benedeczky, I., Timmermans, J. P., Resch, B. A. and Scheuermann, D. W. (1996). Sequential pattern of nerve-muscle contacts in the small intestine of developing human fetus. An ultrastructural and immunohistochemical study. *Histol. Histopathol.* **11**, 845-850.
Garfinkel, A., Tintut, Y., Petrasek, D., Bostrom, K. and Demer, L. L. (2004). Pattern formation by vascular mesenchymal cells. *Proc. Natl. Acad. Sci. USA* **101**, 9247-9250.
Georgieva, R. and Gerov, K. (1975). The morphological and functional differentiation of the alimentary canal of the pig during ontogeny. II. Development and differentiation of the jejunum. *Anat. Anz.* **137**, 16-20.
Gibson, M. C. and Perrimon, N. (2005). Extrusion and death of DPP/BMP-compromised epithelial cells in the developing Drosophila wing. *Science* **307**, 1785-1789.
Gierer, A. and Meinhardt, H. (1972). Theory of biological pattern formation. *Kybernetik* **12**, 30-39.
Goodrich, L. V., Milenkovic, L., Higgins, K. M. and Scott, M. P. (1997). Altered neural cell fates and medulloblastoma in mouse patched mutants. *Science* **277**, 1109-1113.
Hamilton, T. G., Klinghoffer, R. A., Corrin, P. D. and Soriano, P. (2003). Evolutionary divergence of platelet-derived growth factor alpha receptor signaling mechanisms. *Mol. Cell. Biol.* **23**, 4013-4025.
Harfe, B., Scherz, P., Nissim, S., Tian, H., McMahon, A. P. and Tabin, C. (2004). Evidence for an expansion-based temporal Shh gradient in specifying vertebrate digit identities. *Cell* **118**, 517-528.
Harris, M. P., Williamson, S., Fallon, J. F., Meinhardt, H. and Prum, R. O. (2005). Molecular evidence for an activator-inhibitor mechanism in development of embryonic feather branching. *Proc. Natl. Acad. Sci. USA* **102**, 11734-11739.
Hogan, B. L. M. (1996). Bone morphogenetic proteins in development. *Curr. Opin. Genet. Dev.* **6**, 432-438.
Johnson, F. P. (1910). The development of the mucous membrane of the oesophagus, stomach and small intestine in the human embryo. *Am. J. Anat.* **10**, 521-575.
Karlsson, L., Lindahl, P., Heath, J. K. and Betsholtz, C. (2000). Abnormal gastrointestinal development in PDGF-A and PDGFR-(alpha) deficient mice implicates a novel mesenchymal structure with putative instructive properties in villus morphogenesis. *Development* **127**, 3457-3466.
Kedinger, M., Simon-Assmann, P., Bouziges, F., Arnold, C., Alexandra, E. and Haffen, K. (1990). Smooth muscle actin expression during rat gut development and induction in fetal skin fibroblastic cells associated with intestinal embryonic epithelium. *Differentiation* **43**, 87-97.
Keibel, F. and Mall, F. P. (1910). *Manual of Human Embryology*. Philadelphia: J. B. Lippincott Company.
Kolterud, A., Grosse, A. S., Zacharias, W. J., Walton, K., Kretovich, K. E., Madison, B. B., Waghray, M., Ferris, J. E., Hu, C., Merchant, J. L. et al. (2009). Paracrine Hedgehog signaling in stomach and intestine: new roles for hedgehog in gastrointestinal patterning. *Gastroenterology* **137**, 618-628.
Kondo, S. and Miura, T. (2010). Reaction-diffusion model as a framework for understanding biological pattern formation. *Science* **329**, 1616-1620.
Lacroix, B., Kedinger, M., Simon-Assmann, P. and Haffen, K. (1984). Early organogenesis of human small intestine: scanning electron microscopy and brush border enzymology. *Gut* **25**, 925-930.
Li, X., Madison, B. B., Zacharias, W., Kolterud, A., States, D. and Gumucio, D. L. (2007). Deconvoluting the intestine: molecular evidence for a major role of the mesenchyme in the modulation of signaling cross talk. *Physiol. Genomics* **29**, 290-301.
Madison, B. B., Braunstein, K., Kuizon, E., Portman, K., Qiao, X. T. and Gumucio, D. L. (2005). Epithelial hedgehog signals pattern the intestinal crypt-villus axis. *Development* **132**, 279-289.
Maini, P. K. (2004). The impact of Turing's work on pattern fomation in biology. *Math. Today* **40**, 73-92.
Maini, P. K., Baker, R. E. and Chuong, C.-M. (2006). Developmental biology: the Turing model comes of molecular age. *Science* **314**, 1397-1398.
Mathan, M., Moxey, P. C. and Trier, J. S. (1976). Morphogenesis of fetal rat duodenal villi. *Am. J. Anat.* **146**, 73-92.
Matsumoto, A., Hashimoto, K., Yoshioka, T. and Otani, H. (2002). Occlusion and subsequent re-canalization in early duodenal development of human embryos: integrated organogenesis and histogenesis through a possible epithelial-mesenchymal interaction. *Anat. Embryol.* **205**, 53-65.
Meinhardt, H. (2012). Turing's theory of morphogenesis of 1952 and the subsequent discovery of the crucial role of local self-enhancement and long-range inhibition. *Interface Focus* **2**, 407-416.
Mishina, Y., Hanks, M. C., Miura, S., Tallquist, M. D. and Behringer, R. R. (2002). Generation of Bmpr/Alk3 conditional knockout mice. *Genesis* **32**, 69-72.
Mou, C., Pitel, F., Gourichon, D., Vignoles, F., Tzika, A., Tato, P., Yu, L., Burt, D. W., Bed'hom, B., Tixier-Boichard, M. et al. (2011). Cryptic patterning of avian skin confers a developmental facility for loss of neck feathering. *PLoS Biol.* **9**, e1001028.
Muzumdar, M. D., Tasic, B., Miyamichi, K., Li, L. and Luo, L. (2007). A global double-fluorescent Cre reporter mouse. *Genesis* **45**, 593-605.
Nakamura, K. and Komuro, T. (1983). A three-dimensional study of the embryonic development and postnatal maturation of rat duodenal villi. *J. Electron Microsc.* **32**, 338-347.
Rajagopal, R., Huang, J., Dattilo, L. K., Kaartinen, V., Mishina, Y., Deng, C.-X., Umans, L., Zwijsen, A., Roberts, A. B. and Beebe, D. C. (2009). The type I BMP receptors, Bmpr1a and Acvr1, activate multiple signaling pathways to regulate lens formation. *Dev. Biol.* **335**, 305-316.
Raspopovic, J., Marcon, L., Russo, L. and Sharpe, J. (2014). Modeling digits. Digit patterning is controlled by a Bmp-Sox9-Wnt Turing network modulated by morphogen gradients. *Science* **345**, 566-570.
Roberts, D. J., Johnson, R. L., Burke, A. C., Nelson, C. E., Morgan, B. A. and Tabin, C. (1995). Sonic hedgehog is an endodermal signal inducing Bmp-4 and Hox genes during induction and regionalization of the chick hindgut. *Development* **121**, 3163-3174.
Sbarbati, R. (1982). Morphogenesis of the intestinal villi of the mouse embryo: chance and spatial necessity. *J. Anat.* **135**, 477-499.
Shen, J. and Dahmann, C. (2005). Extrusion of cells with inappropriate Dpp signaling from Drosophila wing disc epithelia. *Science* **307**, 1789-1790.
Shyer, A. E., Tallinen, T., Nerurkar, N. L., Wei, Z., Gil, E. S., Kaplan, D. L., Tabin, C. J. and Mahadevan, L. (2013). Villification: how the gut gets its villi. *Science* **342**, 212-218.
Shyer, A. E., Huycke, T. R., Lee, C., Mahadevan, L. and Tabin, C. J. (2015). Bending gradients: how the intestinal stem cell gets its home. *Cell* **161**, 569-580.
Sick, S., Reinker, S., Timmer, J. and Schlake, T. (2006). WNT and DKK determine hair follicle spacing through a reaction-diffusion mechanism. *Science* **314**, 1447-1450.
Trahair, J. and Robinson, P. (1986). The development of the ovine small intestine. *Anat. Rec.* **214**, 294-303.

Development (2016) 143, 427-436 doi:10.1242/dev.130112

Turing, A. M. (1952). The chemical basis of morphogenesis. *Philos. Trans. R. Soc. B Biol. Sci.* **237**, 37-72.

Walton, K. D. and Kolterud, A. (2014). Mouse fetal whole intestine culture system for ex vivo manipulation of signaling pathways and three-dimensional live imaging of villus development. *J. Vis. Exp.* **91**, e51817.

Walton, K. D., Kolterud, A., Czerwinski, M. J., Bell, M. J., Prakash, A., Kushwaha, J., Grosse, A. S., Schnell, S. and Gumucio, D. L. (2012). Hedgehog-responsive mesenchymal clusters direct patterning and emergence of intestinal villi. *Proc. Natl. Acad. Sci. USA* **109**, 15817-15822.

Wells, J. M. and Spence, J. R. (2014). How to make an intestine. *Development* **141**, 752-760.

Zhou, Y., Liu, H.-X. and Mistretta, C. M. (2006). Bone morphogenetic proteins and noggin: inhibiting and inducing fungiform taste papilla development. *Dev. Biol.* **297**, 198-213.

SUPPLEMENTARY MATERIALS AND METHODS

Epithelial-mesenchymal separation

Epithelium was isolated from mesenchyme by mechanical separation following enzymatic treatment with cell recovery solution (BD 354253) as previously described (Madison et al., 2005).

Quantitative RT-PCR

RNA was extracted with Trizol and purified with on column DNase treatment (Qiagen Micro RNeasy) and 1 μg of RNA was used to reverse transcribe cDNA following the standard BioRad iScript protocol. Transcripts were amplified with SYBR green and normalized to the average Cq for 18s rRNA, Rp113a, HPRT and GAPDH. Fold change was calculated as $2^{-\Delta\Delta Cq}$. Primer sets used are listed in Supplemental Table 1.

SEM

Tissues were dissected in 1xPBS on ice and fixed overnight at 4°C in 2.5% glutaraldehyde in Sorenson's phosphate buffer. Three five minute washes in Sorenson's buffer were followed by an ethanol dehydration series (25%, 50%, 70%, 80%, 90%, 100%, 100%) for 15 minutes each. Samples were soaked for two hours in HMDS and then evaporated in a fume hood. Once dry, samples were mounted on carbon tape and cracked with a single edge razor blade to reveal luminal structure. Mounted samples were sputter coated with gold and stored in dessicator until imaging on an AMRAY 1910 field emission scanning electron microscope.

Proliferation index

BrdU was injected into pregnant mothers 2 hours before harvesting fetal intestines as previously described (Walton et al., 2012).

Turing model of pattern formation for mesenchymal clusters in the small intestine of mouse

We have constructed a Turing system comprised of the interactions of two modulators of Bmp signaling, and have systematically tested plausible reactions between these two species. Several parameters are based on previous experimental findings (Walton et al., 2012).

A Turing model describes two morphogens with coupled reaction-diffusion equations, which have the form

$$(1) \qquad \frac{\partial u}{\partial t} = D_u \nabla^2 u + f(u,v)$$

$$(2) \qquad \frac{\partial v}{\partial t} = D_v \nabla^2 v + g(u,v)$$

where u and v are the concentrations of the activator and inhibitor, respectively, D_u and D_v are their constant diffusion coefficients, and $f(u,v)$ and $g(u,v)$ represent the reaction kinetics which are typically nonlinear. In our model, the activator species constitutes a population of molecules that suppresses Bmp signaling and the inhibitor species constitutes a population that promotes Bmp

signaling. In order to address how mesenchymal cells respond chemotactically to this pattern, we write a third differential equation, describing the spatial-temporal distribution of cell density. The rate of change in cell density is given by

$$\frac{\partial N}{\partial t} = \nabla \cdot (D_N \nabla N - \chi N \nabla u) + h(u,v) \quad (3)$$

where D_N is a coefficient for the diffusion-like, random movement of cells and χ is a chemotactic coefficient, which describes how cells respond to the chemical gradient of the activator. In this equation, $h(u,v)$ is a source term governing the net cell population growth rate. The differential equation system (1-3) is closed by specifying the initial and boundary conditions for the chemical species and for the cell population.

Our analysis indicates that the "pure activator-inhibitor" type of reaction kinetics (Dillon and Othmer, 1993) were sufficient to exhibit the spatial patterning of mesenchymal clusters that were qualitatively similar to experimental observations. This particular reaction scheme follows the analysis by Gierer and Meinhardt (Gierer and Meinhard, 1972). For these reactions, we assume a concentration dependent rate for activator species u which is altered by pharmacological inhibitors of Bmp signaling such as dorsomorphin. The reaction rate of u is also inhibited by the presence of v, and there is an additional constant production of u. Both species are subject to degradation, and the inhibitor diffuses more quickly than the activator, i.e. $D_u < D_v$. The reaction terms are then defined as

$$f(u,v) = \lambda \frac{u^2}{v(1+\kappa_u u^2)} - \beta_u u + \alpha \quad (4)$$

$$g(u,v) = \lambda \frac{u^2}{(1+\kappa_v u^2)} - \beta_v v \quad (5)$$

where λ is a scaling factor for the activator-dependent source terms, κ_u and κ_v are constants representing the action threshold for the activator and inhibitor species, respectively, β_u and β_v are the rates of degradation of u and v, respectively, and α represents a constant growth term for u. The net cell population growth rate, $h(u,v)$, is governed by a density-dependent growth rate of the form:

$$h(u,v) = rN \cdot (K - N) \cdot u^2 \quad (6)$$

where r is the net cell division rate and K is the carrying capacity of cells by the tissue. This equation is a modification of the density-dependent logistic population law model, which allows the cell population at time t to depend on the activator concentration (u). By incorporating a carrying capacity, the overall cell population is regulated by its density. If the density is greater than K, the population density rate will be negative, and the density will decrease until it reaches the carrying capacity.

The initial conditions of a spatially uniform steady state were determined by setting the reaction terms equal to zero. Random perturbations localized to the left edge of the domain, corresponding to the anterior end, were induced on this steady state, which initiates a traveling front of pattern formation in

the posterior direction. Simulations were performed in two dimensions on a rectangular grid of size 200x80 (arbitrary units), using no-flux boundary conditions at all edges of the domain in order to mimic the interrupted circularity of the longitudinally cut open intestine. The pattern does not change using cyclic boundary conditions at the edges of the domain to model the closed intestine. A finite element method was used to numerically solve the equations, using a time step of 1/300 and running for 15,000,000 iterations. Parameter values used in all simulations are $\lambda = 0.001$, $\alpha = 0.001$, $\beta_u = 0.02$, $\beta_v = 0.03$, $D_u = 0.02$, $D_v = 1$, $D_N = 0.01$, $\chi = 0.001$, $\kappa_u = 0.02$, $r = 0.000001$, and $K = 10$. These parameters were previously used by Dillon and Othmer (Dillon and Othmer, 1993), with minor adjustment for this specific system. The parameters are within the constraints set up by Gierer and Meinhardt (Gierer and Meinhard, 1972) for pattern formation models with 'pure activator-inhibitor' systems.

By altering the concentration-dependent action threshold for the activator species through varying values of κ_v, this mechanism recapitulates the experimentally observed patterns, shown in Figure 9. In the absence of dorsomorphin ($\kappa_v = 0.06$), the activator's action threshold is below that of the inhibitor and a spotted pattern is produced (Fig. 9A). Moderate concentrations of dorsomorphin ($\kappa_v = 0.09$) evoke larger and paddle-like fusion of clusters (Fig. 9C). At high concentrations of dorsomorphin ($\kappa_v = 0.11$), the system evolves into a striped pattern (Fig. 9B). We also observe that upon allowing the pattern to fully develop at low values for the action threshold of activator species, a step-wise increase in the activator concentration causes the computed spotted pattern to evolve into a striped pattern (see Figure 9I, 9J and Supplemental Movie 2).

We also extended our investigation to account for a Bmp bead (see Figures 4 and S2), which was represented as a spatially restricted source of the inhibitor (which promotes Bmp signaling). This was done by adding an expression for the circular bead to the existing source term for the inhibitor

$$(7) \qquad g(u,v) = \lambda \frac{u^2}{(1+\kappa_v u^2)} - \beta_v v + \exp\left[-\left((x-x_b)^2 + (y-y_b)^2\right)\right]$$

where x_b and y_b indicate the position of the bead, placed in the center of the domain. Our results, shown in Figure 9D, confirm that sites of high concentration of the activator species, indicative of Bmp inhibiting clusters, do not form in the region surrounding the bead.

This demonstrates that the interactions between an activator and inhibitor of Bmp signaling can explain the localized mesenchymal clustering preceding villus formation in the mouse. Other effects may influence the Turing field of Bmp activators and inhibitors, such as domain growth in the rapidly expanding developmental intestine.

REFERENCES

Blank, U., Seto, M., Adams, D., Wojchowski, D., Karolak, M. and Oxburgh, L. (2008). An in vivo reporter of BMP signaling in organogenesis reveals targets in the developing kidney. *BMC Dev Biol* **8**, 86.

Dillon, R. and Othmer, H. G. (1993). Control of Gap Junction Permeability Can Control Pattern-Formation in Limb Development. *Experimental and Theoretical Advances in Biological Pattern Formation* **259**, 65-81.

Gierer, A. and Meinhard, H. (1972). Theory of Biological Pattern Formation. *Kybernetik* **12**, 30-39.

Haramis, A. P., Begthel, H., Van Den Born, M., van Es, J., Jonkheer, S., Offerhaus, G. J. and Clevers, H. (2004). De novo crypt formation and juvenile polyposis on BMP inhibition in mouse intestine. *Science* **303**, 1684-1686.

Madison, B. B., Braunstein, K., Kuizon, E., Portman, K., Qiao, X. T. and Gumucio, D. L. (2005). Epithelial hedgehog signals pattern the intestinal crypt-villus axis. *Development* **132**, 279-289.

Shyer, A. E., Huycke, T. R., Lee, C., Mahadevan, L. and Tabin, C. J. (2015). Bending gradients: how the intestinal stem cell gets its home. *Cell* **161**, 569-580.

Walton, K. D., Kolterud, A., Czerwinski, M. J., Bell, M. J., Prakash, A., Kushwaha, J., Grosse, A. S., Schnell, S. and Gumucio, D. L. (2012). Hedgehog-responsive mesenchymal clusters direct patterning and emergence of intestinal villi. *Proc Natl Acad Sci U S A* **109**, 15817-15822.

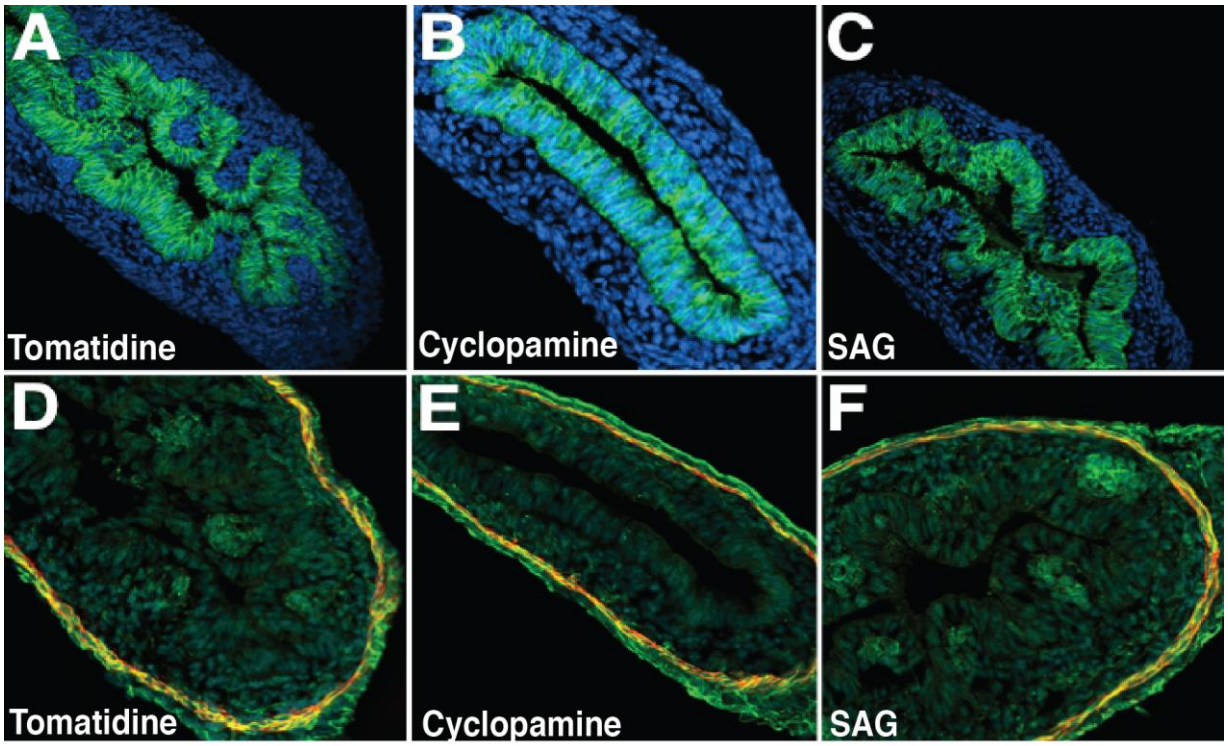

Fig. S1. Perturbing Hh signaling changes cluster patterning, but does not alter smooth muscle. Intestines were harvested at E13.5 and treated for two days in transwell culture. A,D) Control intestines treated with tomatidine; B,E) treated with cyclopamine to block Hh signaling; C,F) treated with SAG to increase Hh signaling. A-C) stained with anti-E-cadherin (green) to show villus emergence and DAPI (blue). D-F) stained with desmin (green) to show smooth muscle precursor cells and alpha-smooth muscle actin (red) to show mature smooth muscle. A-C are reprinted with permission from Walton et al., 2012; D-F are serial sections from the same tissues as A-C. Also note that the cross sections are approximately the same caliber, suggesting that the degree of confinement of the epithelium by the muscle is similar in all cases.

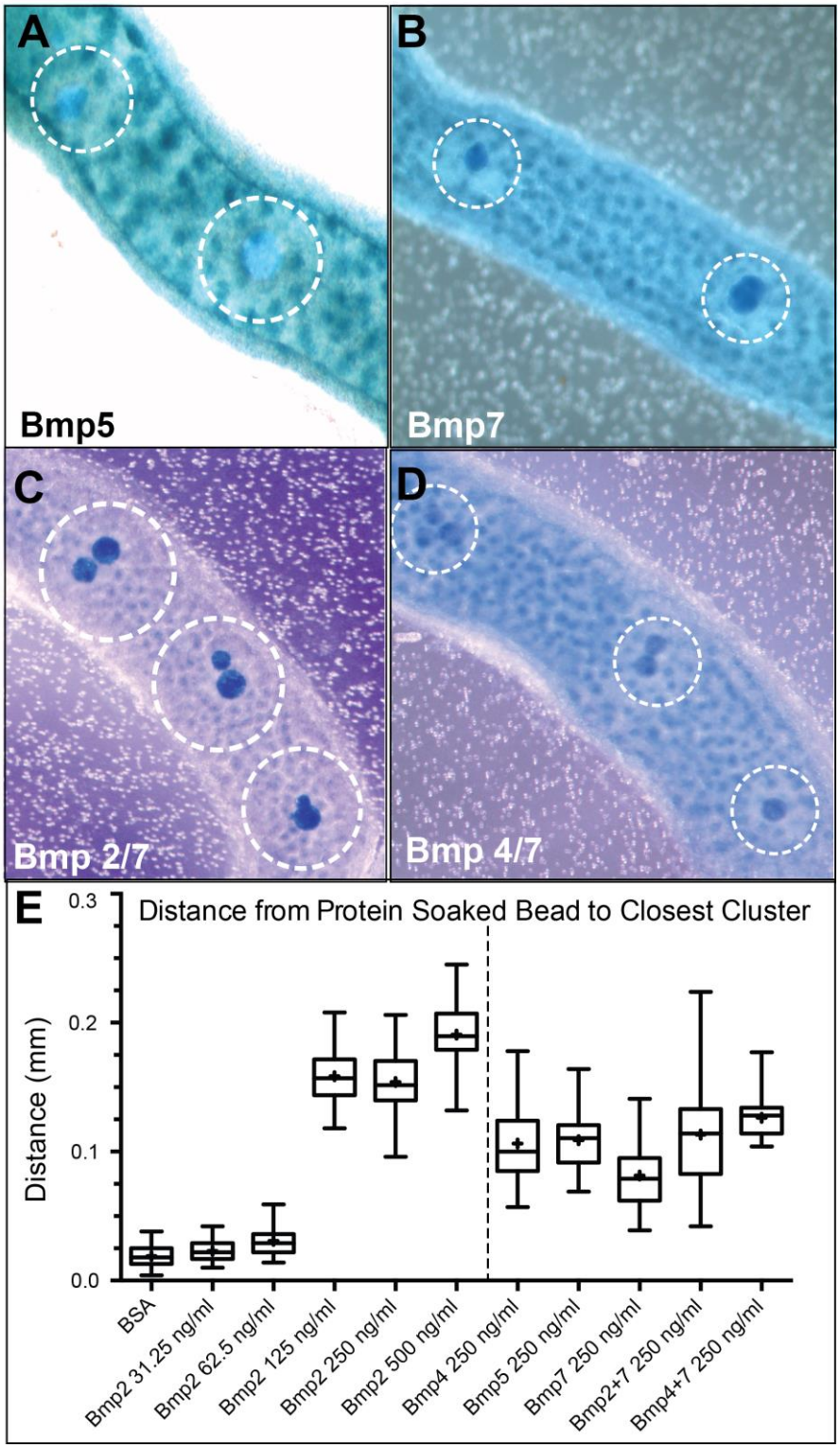

Fig. S2. Wholemount Xgal staining of $Ptc^{LacZ/+}$ E13 intestines cultured for 2 days with agarose beads soaked with Bmp recombinant proteins (250 ng/ul from R&D Systems). Hatched circles outline the area of clearing around the beads; faint clusters within the hatched circles are on the opposite/abluminal side from the beads (similar to Figure 4). At least 5 beads were placed on 3 different intestines for each

bead type; this was repeated at least 3 times. Panel E are Box and Whiskers plots of the average distance measured from the edge of the bead to the closest clusters. Boxes contain the median and quartiles and whiskers show the high and low. Mean is represented by the + inside each box. The left of the dashed line shows a concentration curve for Bmp2. The right side of the dashed line shows the clearing around the other Bmp ligand beads.

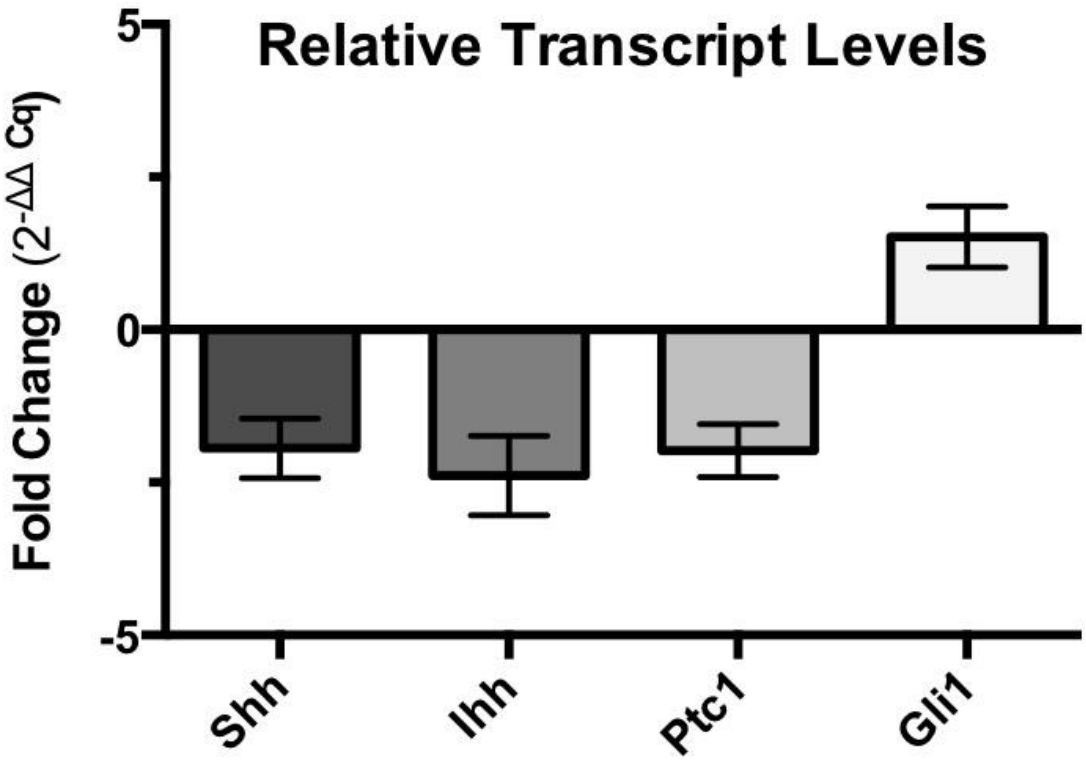

Fig. S3. Inhibition of Bmp signaling does not alter the expression of Hedgehog ligands or targets. Quantitative PCR of E13.5 intestines treated with dorsomorphin (20 μm) for two days versus E13.5 control intestines treated with DMSO for two days. Each sample was pooled from 3 intestines (9 samples total for each condition). Bars represent change in relative transcript levels calculated for Shh, Ihh Ptc1 and Gli1. Error bars are the standard of deviation between three independent samples. Transcript levels were not significantly different for Shh, Ihh, Ptc1 or Gli1 (Mann-Whitney test p-values 0.0142, 0.1128, 0.0142, 0.160).

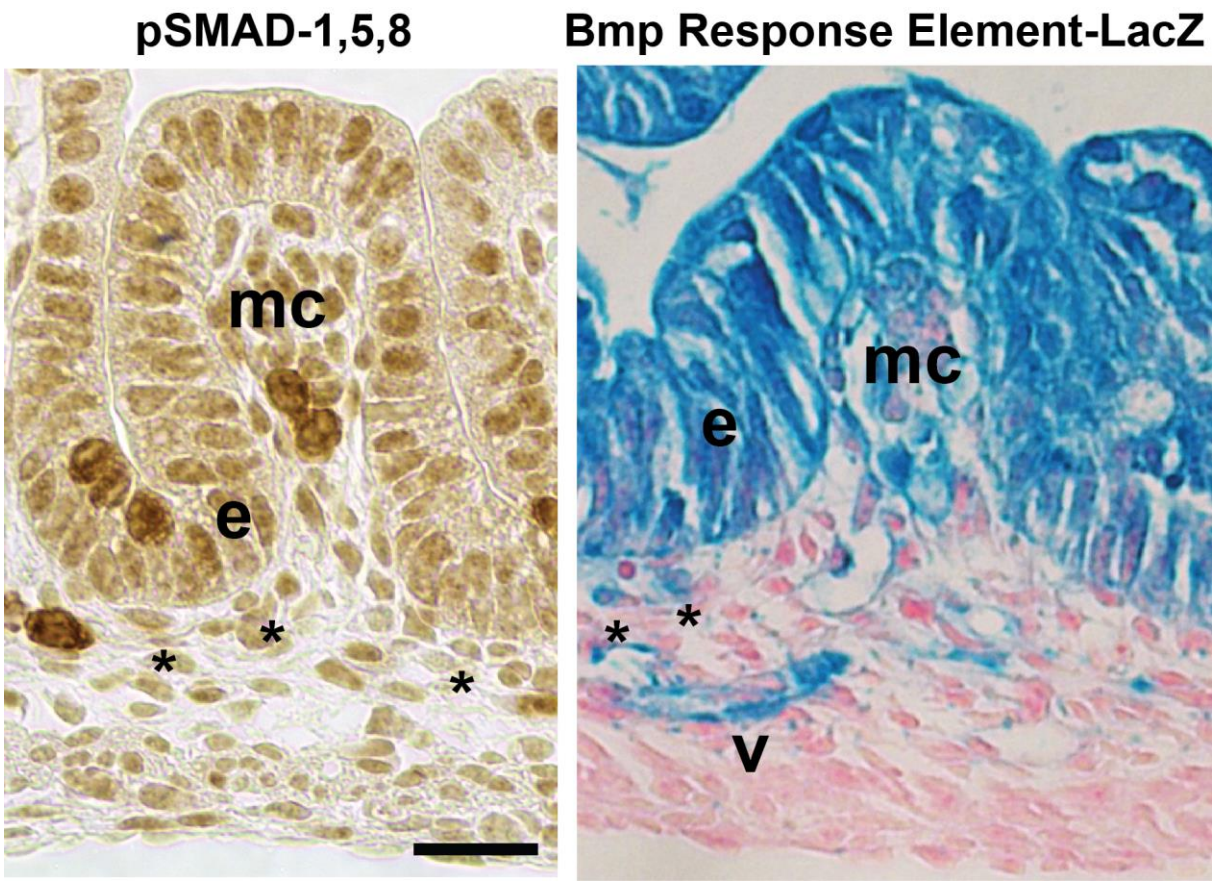

Fig. S4. Bmp signaling at E15.5 is detected in the epithelium (e), and mesenchyme in the mesenchymal clusters (mc), sub-epithelial myofibroblasts (*), and vasculature (v) reported by x-gal staining in BRE-LacZ intestines (blue; A, C) and p-SMAD 1,5,8 immunostaining (brown, B,D). BRE-LacZ mice were described previously (Blank et al., 2008).

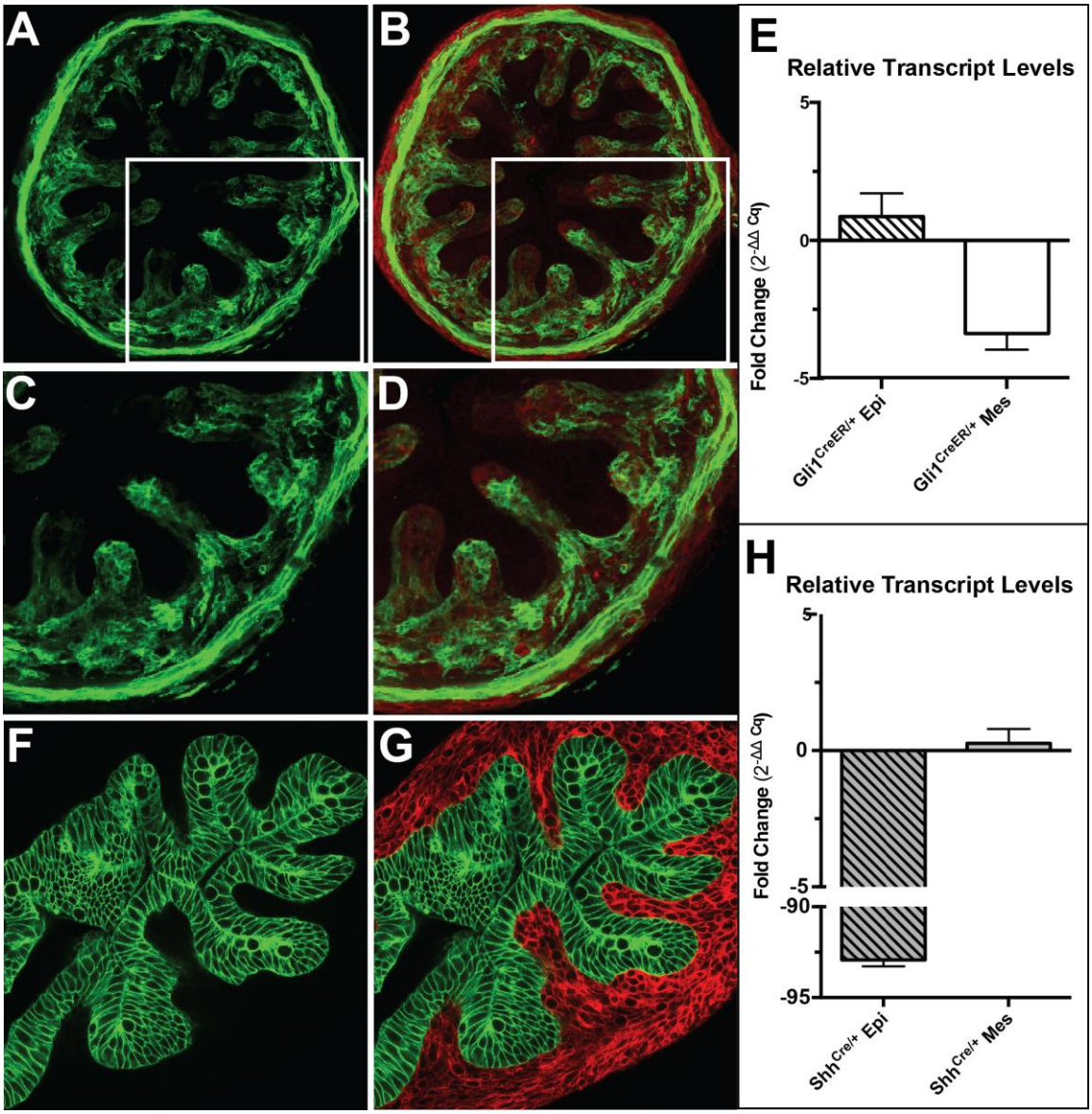

Fig. S5. Mesenchymal and epithelial specific recombination of conditional alleles in mT/mG reporter intestines at E15.5 with Gli1^{CreERT2} (A-E) or Shh^{Cre} (F-H). C and D are magnifications of the boxed areas in A and B, respectively. Green shows recombined cells. Relative Bmpr1a transcript levels measured by quantitative PCR in epithelium or mesenchyme separated from Bmpr1af/f; Gli1CreER/+ intestines versus Bmpr1a$^{f/f}$; Gli1$^{+/+}$ intestines (E) or Bmpr1a$^{f/f}$; Shh$^{CreER/+}$ intestines (F). At least three different samples were tested for each tissue of each genotype and each sample was pooled from 3 intestines (9 intestines total for each genotype). Samples were tested in triplicate and normalized to the average of 4 standardization transcripts (18s rRNA, Rp113a, HPRT and GAPDH). Bars represent fold change. Error bars are the standard of deviation between the three different samples. In epithelial conditional mutants, Bmpr1a transcripts were significantly decreased in the epithelium (92.9 fold; p= 0.0006), but not in the mesenchyme (0.266 fold; p=0.023). In mesenchymal conditional mutants, Bmpr1a transcripts were decreased in the mesenchyme (3.37 fold) though this was not statistically different from transcripts levels in control mesenchyme (p= 0.104); epithelial transcript levels were not significantly decreased (0.869 fold; p= 0.700).

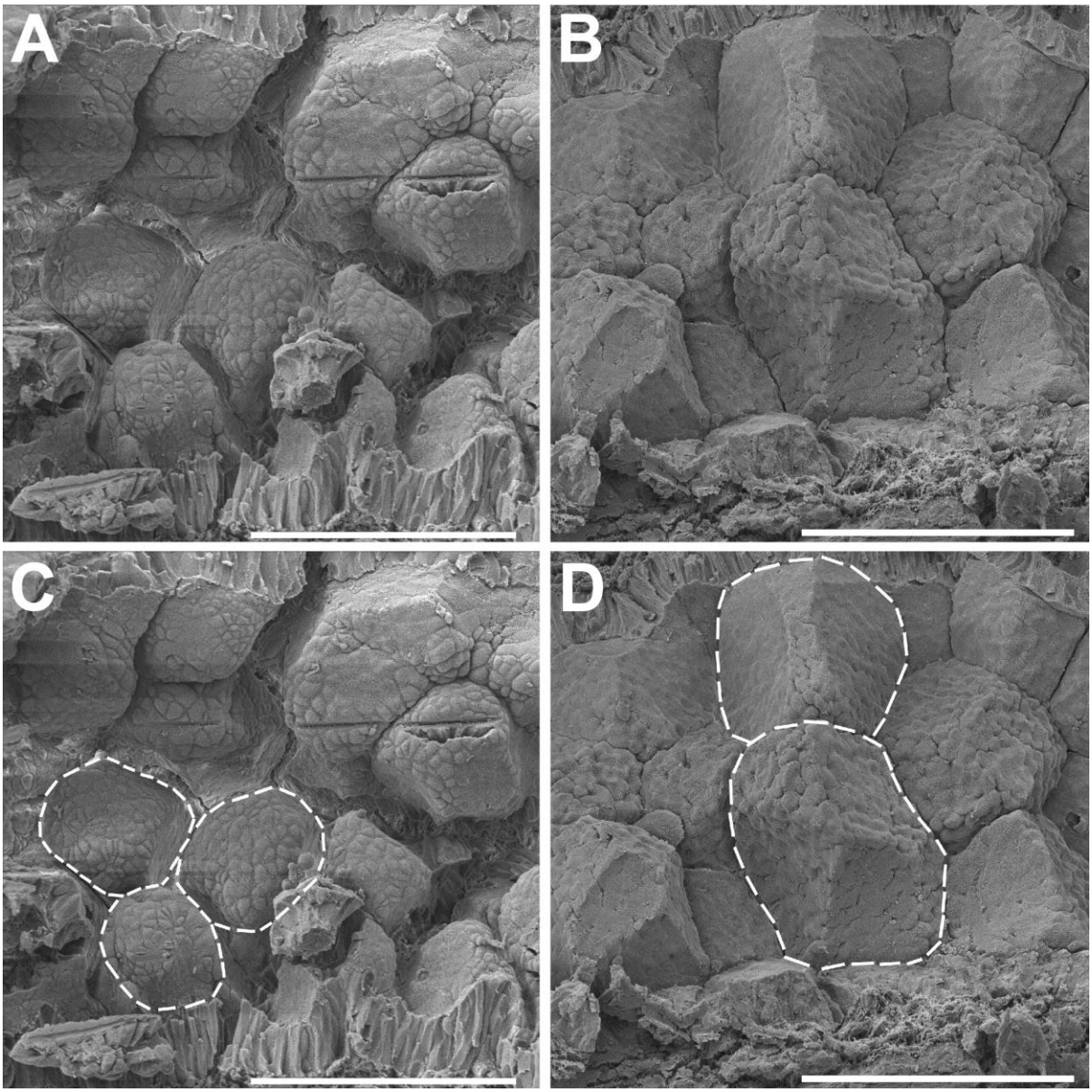

Fig. S6. Large merged clusters are detected by scanning electron microscopy in Bmpr1a mutant intestines at E15.5. A) Control littermate jejunum. B) Bmpr1a$^{f/f}$; Gli1$^{CreER/+}$ mutant jejunum. C and D are the same images as in A and B; white cross-marks highlight individual villi and emphasize size and shape differences. Thirteen mutant intestines and four control littermates were examined. Scalebars are 100 μm.

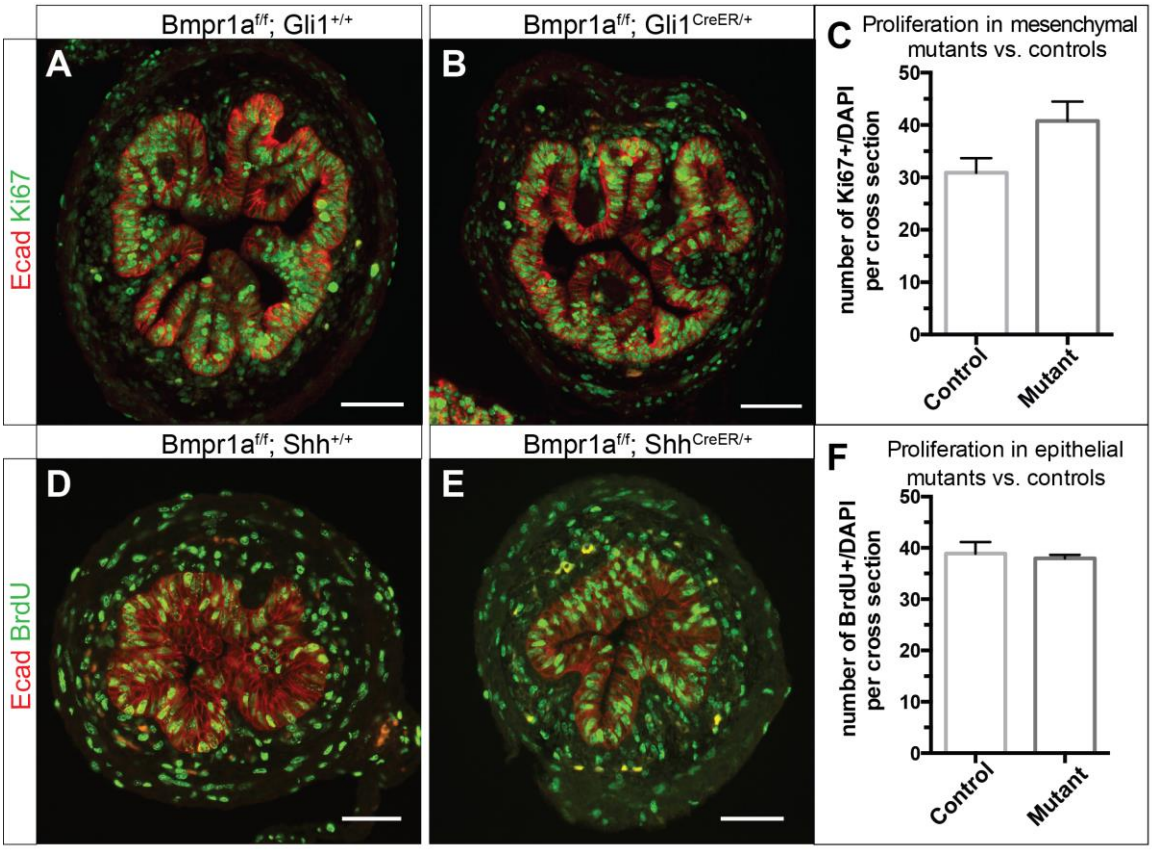

Fig. S7. Mesenchymal loss of Bmpr1a results in increased proliferation. Bmp signaling regulates proliferation in a variety of settings and overexpression of the Bmp inhibitor, noggin, in the postnatal intestine increases epithelial proliferation (Haramis et al., 2004). We therefore examined proliferation in our mutant mice. The index of proliferation was measured by the ratio of Ki67+ cells or BrdU+ cells to DAPI+ nuclei. Epithelium is outlined by E-cadherin staining. A-C) Mesenchymal proliferation (Ki67 index) was increased by 30% in Bmpr1a$^{f/f}$; Gli1$^{CreER/+}$ mesenchymal mutants compared to Bmpr1a$^{f/f}$; Gli1$^{+/+}$ control littermates (p= 0.029; Mann-Whitney test). D-F) Surprisingly, proliferation (BrdU index) in Bmpr1a$^{f/f}$; Shh$^{Cre/+}$ epithelial mutants was not different from their control Bmpr1a$^{f/f}$; Shh$^{+/+}$ littermates (p= 0.857; Mann-Whitney), however the notion that the effect of Bmp on regulation of intestinal epithelial proliferation might differ in fetal versus postnatal life has been previously raised (Madison et al., 2005). It should also be noted that while increased proliferation will allow the Turing model to reach saturating conditions more quickly, the pattern will not be altered. Bargraphs in C and F show the average index with standard deviation. Scalebars are 50 μm.

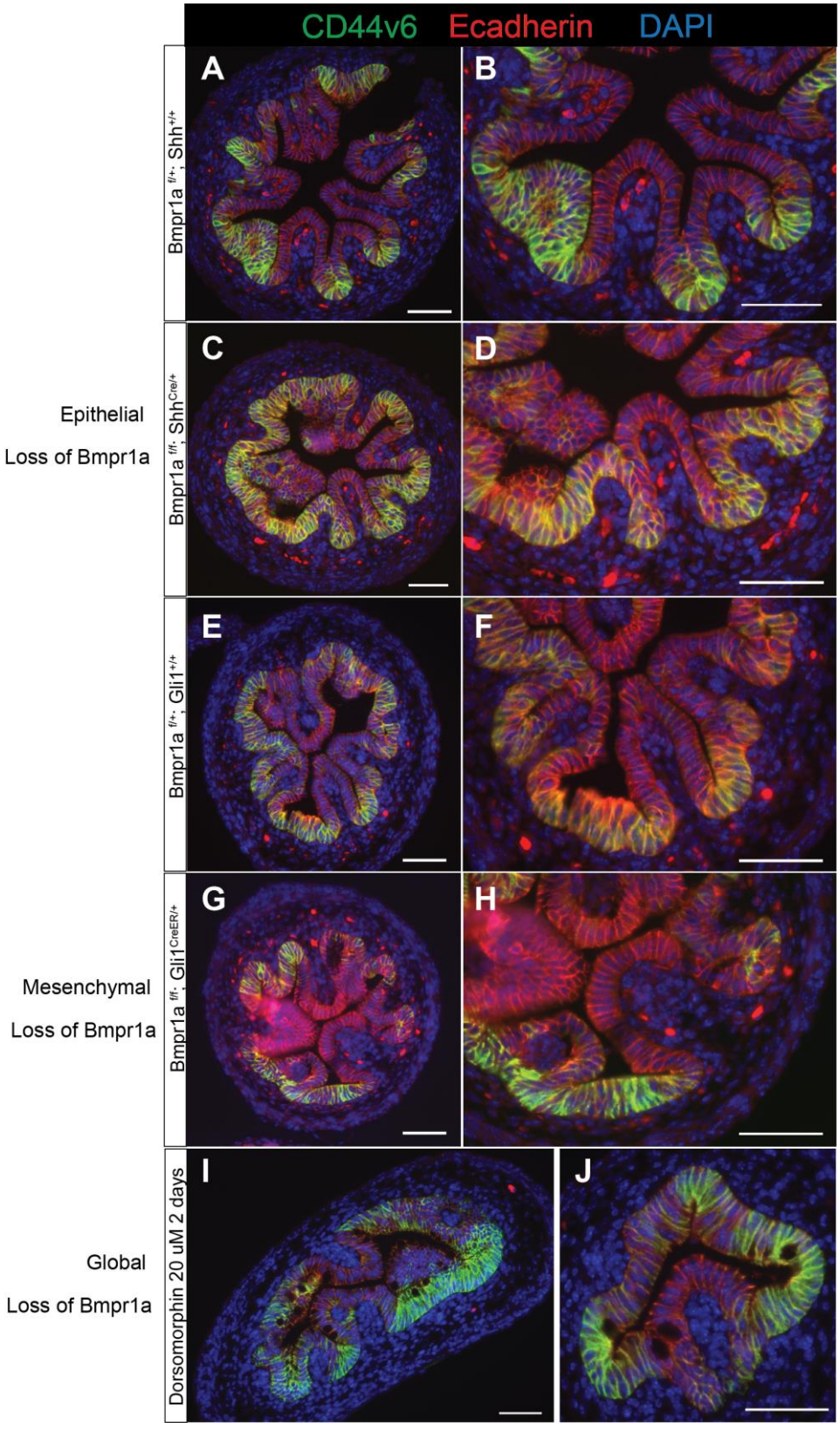

Fig. S8. Wnt signaling is not changed when Bmp signaling is altered. Because the Wnt target gene, CD44v6, becomes restricted to the intervillus regions during villus outgrowth (Madison et al., 2005; Shyer et al., 2015), we examined whether altered epithelial bending in mesenchymal cluster mutants

would affect the restriction of Wnt responsive cells to the intervillus regions. At E15.5, no obvious changes in CD44v6 restriction were seen. A-D) CD44v6 staining in control (A,B) vs. epithelial Bmpr1a mutants (C,D) showing the full cross-section (A,C) and magnified panels (B,D). E-H) CD44v6 staining in control (E,F) vs. mesenchymal Bmpr1a mutants (G,H) showing the full cross-section (E,G) and magnified panels (F,H). I) CD44v6 staining in E13.5 intestines treated for 2 days with 20 μm dorsomorphin. J) Magnification of I. E-cadherin outlines the epithelium. Scalebars are 50 μm.

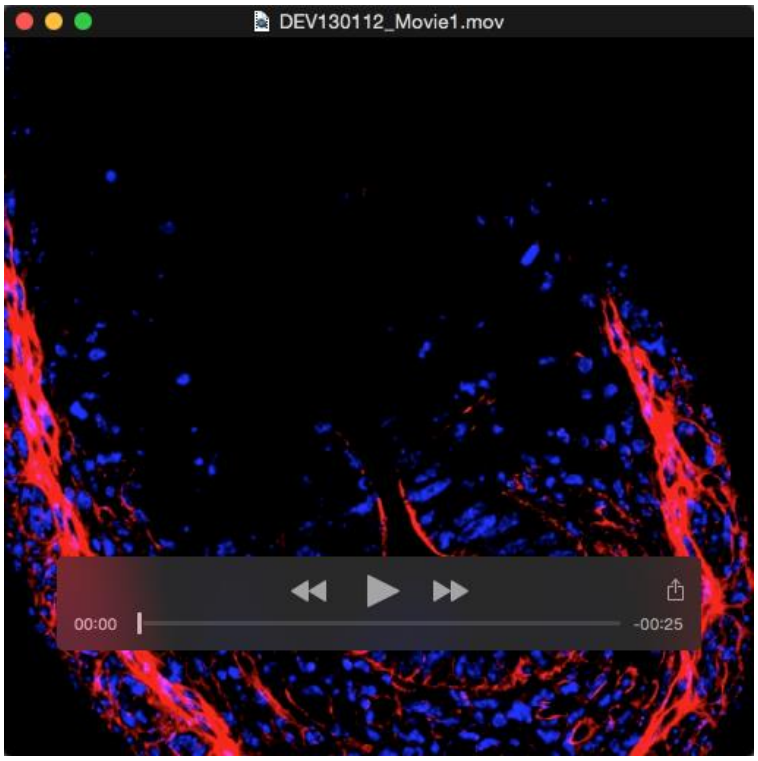

Movie 1. Mesenchymal clusters are associated with basal deformation of the epithelium. This movie steps through optical sections of the z-stack; mesenchymal clusters associated with epithelial deformations may appear hidden unless visualized in three dimensions or in a z stack such as this. Note the basal deformation in the presence of a flat apical surface.

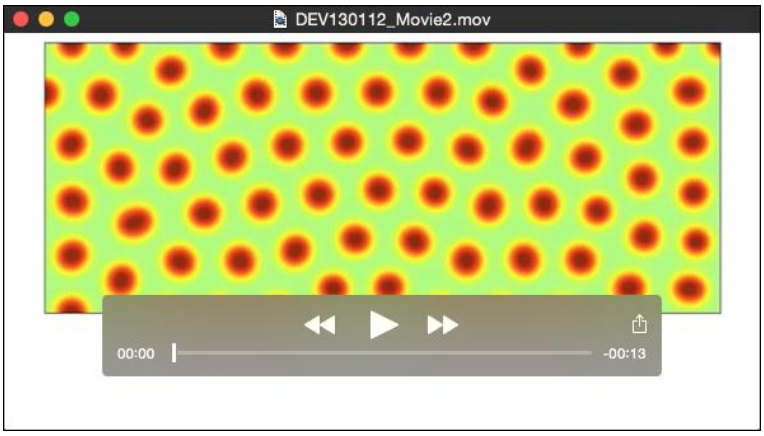

Movie 2. The movie starts with a field of clusters in a Turing field that have developed under normal conditions until clusters form. The movie follows the field pattern as the concentration of activator is increased to saturation; clusters begin to merge to become stripes.

Table S1. RT-PCR primers.

Click here to Download Table S1